ANALYSIS OF RECONFIGURABLE ANTENNA WITH MOVING PARASITIC ELEMENTS

by

Xu Han
B.Sc. Nanjing University of Information Science & Technology, 2007

THESIS SUBMITTED IN PARTIAL FULFILLMENT OF
THE REQUIREMENTS FOR THE DEGREE OF

MASTER OF APPLIED SCIENCE

In the
School of Engineering Science

© Xu Han 2010

SIMON FRASER UNIVERSITY

Fall 2010

All rights reserved. However, in accordance with the *Copyright Act of Canada*, this work may be reproduced, without authorization, under the conditions for *Fair Dealing*. Therefore, limited reproduction of this work for the purposes of private study, research, criticism, review and news reporting is likely to be in accordance with the law, particularly if cited appropriately.

APPROVAL

Name: **Xu Han**

Degree: **Master of Applied Science**

Title of Thesis: **Analysis of Reconfigurable Antenna with Moving Parasitic Elements**

Examining Committee:

Chair:

_____

Dr. Paul Ho, P. Eng.
Professor, School of Engineering Science

_____

Dr. Rodney Vaughan
Senior Supervisor
Professor, School of Engineering Science

_____

Dr. Carlo Menon, P. Eng.
Supervisor
Assistant Professor, School of Engineering Science

_____

Dr. Shawn Stapleton, P. Eng.
Internal Examiner
Professor, School of Engineering Science

Date Defended/Approved: September 13, 2010

SFU SIMON FRASER UNIVERSITY
LIBRARY

Declaration of
Partial Copyright Licence

The author, whose copyright is declared on the title page of this work, has granted to Simon Fraser University the right to lend this thesis, project or extended essay to users of the Simon Fraser University Library, and to make partial or single copies only for such users or in response to a request from the library of any other university, or other educational institution, on its own behalf or for one of its users.

The author has further granted permission to Simon Fraser University to keep or make a digital copy for use in its circulating collection (currently available to the public at the "Institutional Repository" link of the SFU Library website <www.lib.sfu.ca> at: <http://ir.lib.sfu.ca/handle/1892/112>) and, without changing the content, to translate the thesis/project or extended essays, if technically possible, to any medium or format for the purpose of preservation of the digital work.

The author has further agreed that permission for multiple copying of this work for scholarly purposes may be granted by either the author or the Dean of Graduate Studies.

It is understood that copying or publication of this work for financial gain shall not be allowed without the author's written permission.

Permission for public performance, or limited permission for private scholarly use, of any multimedia materials forming part of this work, may have been granted by the author. This information may be found on the separately catalogued multimedia material and in the signed Partial Copyright Licence.

While licensing SFU to permit the above uses, the author retains copyright in the thesis, project or extended essays, including the right to change the work for subsequent purposes, including editing and publishing the work in whole or in part, and licensing other parties, as the author may desire.

The original Partial Copyright Licence attesting to these terms, and signed by this author, may be found in the original bound copy of this work, retained in the Simon Fraser University Archive.

Simon Fraser University Library
Burnaby, BC, Canada

ABSTRACT

Many communications applications require antennas with beam-steering ability and diversity performance. A new reconfigurable antenna is proposed and analyzed. It comprises moving parasitic elements near an active element. As a result of the changing mutual coupling between the parasitic elements and the active element, the antenna pattern changes. By carefully arranging the shape and locus of the parasitic elements, the impedance remains matched. This design has promising pattern-changing ability and is demonstrated to be capable of good diversity performance. By keeping the active element stationary, metal fatigue is eliminated and the reliability of such a mechanical system is improved. A parametric study is undertaken by simulation using commercial software. The diversity performance is evaluated using pattern correlation functions. The accuracy of the simulation software is also checked using canonical antenna configurations, namely the dipole. The results also demonstrate the advantages and limitations of different commercial simulation software.

Keywords: antennas; reconfigurable antenna; beam-steering; pattern correlation; parasitic elements; dipole.

ACKNOWLEDGEMENTS

In my graduate studies, I have accepted enormous help from many people, especially my senior supervisor, Dr. Rodney G. Vaughan. I am very grateful for his complete support in both my research and life. I would like to thank him for all his guidance, support and encouragements. My research will not be accomplished without him.

I am indebted to many of my lab colleagues, past and present. For their encouragement, help and advice during these years. Special thanks to Jinyun Ren, Jane X. Yun, Qi Yang. My thesis will not be possible without them.

I am honored to thank my committee members, Dr. Shawn Stapleton and Dr. Carlo Menon; and the chair of my defense, Dr. Paul K.M. Ho, for their valuable contributions.

Finally, I would like to express my deepest thanks to my parents, family and friends. They provide years of care, encouragement, and support throughout my life and studies.

TABLE OF CONTENTS

LIST OF FIGURES

LIST OF TABLES

GLOSSARY

RF	Radiofrequency
MIMO	Multiple-input and multiple-output
SISO	Single-input and single-output
MEA	Multi-Element Antenna
MoM	Method of Moments
FEM	Finite Element Method
FDTD	Finite Difference Time Domain
pdf	Probability density function

LIST OF SYMBOLS

Z_{dipole}	Impedance of a dipole antenna
$Z_{monopole}$	Impedance of a monopole antenna
$Y_{monopole}$	Admittance of a monopole antenna
$a_{monopole}$	Radius of a monopole antenna
Z_0	Free space impedance
k	Wave number
$L_{monopole}$	Length of a monopole antenna
γ	Euler constant
$R_{monopole}$	Resistance of a monopole antenna
$X_{monopole}$	Reactance of a monopole antenna
α	Parasitic element rotating angle
β_v	Bend angle of the V-Shaped parasitic element
L_v	Total length of the V-Shaped parasitic element
R	Groundplane length/width
d	Distance between the active and parasitic elements
$S(\theta,\varphi)$	Probability density function of the incident waves
$E(\theta,\varphi)$	Far-field pattern of the antenna pattern
ρ_{12}	Correlation coefficient of two patterns
β_{shell}	Shell angle of the Shell-Shaped parasitic element
L_{shell}	Length of the Shell-Shaped parasitic element

1: INTRODUCTION

In mobile communications, the antenna plays a critical role in transmitting and receiving signal from one terminal to another. The antenna was introduced by Heinrich Hertz in 1888. Physically composed of one or more conductors (sometimes with dielectric), the antenna can work as both transmitter and receiver. In the transmit mode, the radiofrequency (RF) current is generated at the antenna terminal, causing the antenna to radiate and generate an electromagnetic field. For the receive mode, the electromagnetic field from another source induces a voltage and corresponding current at the antenna's terminal.

Multi-input, multi-output (MIMO) has attracted great research attention in wireless communications since its concept became popular in the 1990s. The performance gain of MIMO looks promising when compared with single-input, single-output (SISO). However, the performance gain, such as the diversity gain, is compromised if the mutual coupling between adjacent antenna elements is too high. In particular, a high diversity gain is very difficult to achieve for most popular wireless devices because the devices are compact and provide limited space for antennas.

In this thesis, we propose a new, reconfigurable antenna using parasitic elements in close proximity of a monopole antenna. The mutual coupling between the parasitic and the active monopole enable diversity action, and the antenna is classed as a type of reconfigurable antenna. The diversity performance is evaluated using pattern correlation techniques within commercial simulation packages.

1.1 Motivation

Classically, arrays and steerable reflectors are used for high directivity beam steering, but arrays and MEAs (Multi-Element Antenna) are also used for low pattern directivity applications such as diversity/MIMO for communications in wide-angular spread multipath. A method to reduce the cost of a full array/MEA, with its full complement of front-end electronics, is to use changeable reactive loading on parasitic elements.

Dipole configurations, e.g., [1],[2] and monopole ones e.g., [3],[4] have been developed for beam-steering, and also switched parasitic patch antennas have been used [5],[6]; including designs for diversity/MIMO [7]. The designs include implementation as monopoles on a finite groundplane, e.g., [8]. The switched parasitic approach introduces the practical advantage of fewer front-end chains at the expense of constrained performance. A disadvantage is that the electronic switches, such as PIN diodes, or switches, can introduce

nonlinearities, with associated communications performance degradation on receive and spectral violations on transmit. In this thesis, we use mechanical movement of an isolated parasitic element to get round this problem.

More recently, there has been interest in mechanically actuated antennas for adapting to changing requirements or conditions, e.g. [9],[10]. This is not an intuitively obvious direction from the viewpoint of re-introducing long-deposed mechanical reliability issues, and the need for the actuation hardware, power supply, and control electronics. For a fair comparison, these components need to be included in a volumetric comparison to judge the compactness and effectiveness of designs. Moreover, mechanical pattern changes are slow and do not have the agility or beam-forming ability of an electronic array for a similar volume or aperture. Nevertheless, new technology is emerging which looks promising for low cost mechanically actuated systems, justifying a new look at mechanical/mechatronic approaches. For example, in [11], an electroactive polymer is used to demonstrate pattern changes using a single moving parasitic element. In this thesis, we look to a more sophisticated design using multiple moving parasitic elements.

1.2 Choice of Simulation Software

The performance of the reconfigurable antenna is evaluated by commercial simulation software packages. However, even for the most well-known monopole

antenna, different software packages yield various results, especially for the impedance. Since there are seldom theoretical impedance results for new designs, it is a problem to choose the best software package for the simulation.

To overcome this problem, we compare the impedance results for the basic elementary dipole antennas in different dimensions using various simulation software packages. Other analytical methods, as well as physical measurement results, are also employed to confirm the simulation accuracy.

Traditionally, numerical methods such as the Method of Moments (MoM) [12], and analytic methods such as the Wave-Structure Method [13] and the induced EMF method [14] are used to calculate a dipole antenna impedance. The Method of Moments is classically specialized for wires with an electrically small radius, commonly defined as less than 0.01λ [15]-[17]. Beyond this range, the assumptions of the method begin to breakdown. However, extended approaches have been proposed to increase the impedance accuracy of the dipole antenna with larger radius, e.g., [18], [19]. Here, the authors claimed a reasonable impedance result compared to the measurement result for a dipole antenna with a radius of 0.1129 λ and different antenna lengths or feeding gap sizes. But their simulation results still show a 20%-30% difference from the measurement. On the other hand, the Wave-Structure method provides solutions to semi-infinite wire antennas, producing the impedance results related to both antenna length and thickness. But the results turn out to be accurate only for short lengths, e.g., monopoles which are less than about 0.2 wavelengths long.

The commercial simulation software packages, e.g. HFSS, CST and WIPL-D, are much more powerful and versatile in handling different applications. Each of them is based on a different fundamental mathematic method, such as Method of Moments, Finite Element Method (FEM) [20], Finite Difference Time Domain (FDTD) [21]-[23]. The resulting simulated impedances, for the same antenna, are significantly different for these different approaches.

After confirming the accuracy of the software packages by comparing the results with analytical methods and measurement results, the diversity performance of the reconfigurable antenna was investigated in terms of the pattern correlations. We successfully developed reconfigurable antennas with high diversity gain.

1.3 Thesis Outline

This thesis is structured as follows. Chapter 2 introduces the electromagnetic simulation software packages, and in order to choose an appropriate simulation package for the reconfigurable antenna, various simulations are performed and compared with analytical and measurement results.

In Chapter 3, the proposed reconfigurable antenna is presented and discussed, including pattern correlations. The advantage is that the active RF element in the model is stationary, which reduces the complexity.

Chapter 4 reviews another type of reconfigurable antenna by employing a new shape of parasitic element - composed of movable metal sheets instead of wire. The results shown even better diversity performance (better pattern decorrelation).

Finally, Chapter 5 summarizes the research work in this thesis and provides suggestion for related future work.

1.4 Contribution of the Thesis

A new type of the reconfigurable antennas for diversity is developed. Unlike other diversity antennas, this particular type of antenna has no moving parts in the active RF path, so the RF feeding circuit remains stationary, eliminating the possibility of metal fatigue and increasing the reliability of such a mechanical system.

One of the advantages for this model is the good pattern-changing ability. The radiation pattern changes quickly with the rotation of the parasitic elements, giving good diversity performance. The results show that even a small rotation of the parasitic elements will lead to a significant reduction in the correlation

coefficient function. Moreover, by carefully arranging the shape and locus of the parasitic elements, the impedance remains matched.

Such an antenna has promising applications. It could be useful for base stations or wireless network devises which operate in slow changing multipath environments. Furthermore, if the frequency is dramatically increased, e.g., to 60GHz (used for short distance wireless connections), the antenna dimensions are reduced to a scale suitable for implementation on chips.

Moreover, a comprehensive verification is performed since no theoretical impedance results exist for dipole antenna under practical dimensions. After the investigation of each simulation software, they are categorized into different classes. For future simulations, the appropriate software can be selected according to the class of antenna.

2: SIMULATION SOFTWARE COMPARISON AND SELECTION

To evaluate accurately the performance of reconfigurable antennas, a suitable simulation package is required. Many kinds of electromagnetic simulation packages are available, such as HFSS, CST and WIPL-D. Each of them utilizes fundamentally different mathematical method, causing the simulated results to be different, especially for the impedance. The radiation patterns simulated by those packages, on the other hand, are usually similar. It is therefore necessary to verify the impedance results of each package before applying them to performance evaluation of the reconfigurable antennas.

In this chapter, we use HFSS, CST and WIPL-D to simulate the impedance of a basic dipole antenna. We discuss the accuracy of the Induced EMF Method and Wave-Structure Method. The measured dipole impedance results are also used for the comparison.

This chapter starts with a brief introduction to the simulation packages in Section 2.1. Theoretical dipole impedance results are discussed in Section 2.2.

The impedance verification results are in Section 2.3. The conclusion is in Section 2.4.

2.1 Simulation Packages Introduction

Some wire dipole configurations are investigated using the different packages.

2.1.1 HFSS

HFSS, introduced by Ansoft, is a very popular and powerful simulation package for electromagnetic solutions. It utilizes the Finite Element Method to create mesh grids around the model and solves for a given frequency. The results prove that HFSS is versatile for most configurations. However, there are also some disadvantages. Firstly, the stability of the software is not very good when calculating large-sized, intricate structures. Secondly, the creation of the feeding port is complicated compared with other software.

2.1.2 CST

CST stands for Computer Simulation Technology and consists of Microwave Studio, EM Studio, PCB Studio, etc. We focus on the Microwave Studio which employs the Finite Difference Time Domain Method. The method is

based on the time domain and can cover a wide frequency band with one single simulation run. It is also quick and suitable for non-uniform models. However, results from CST do not closely fit for configurations with a large range of dimensions, such as a half wavelength dipole using an impractically thin wire for example. This is because of CST's sensitivity to extremely small mesh grid settings.

2.1.3 WIPL-D

The WIPL-D results are from an older (than is currently sold) version that employs only the traditional Method of Moments, This method is particularly suitable for wire antennas with impractically thin conductors. However, this software package becomes inaccurate for some practical configurations, such as a fat dipole.

2.2 Theoretical Dipole Impedance

The theoretical impedance for a thin, half-wavelength dipole antenna is given in [24] as

$$Z_{dipole} = 73.13 + j42.35\Omega \quad \textbf{(3-1)}$$

For the equivalent monopole antenna on a infinite groundplane, the impedance is half of the dipole antenna:

$$Z_{monopole} = 36.57 + j21.18\Omega \quad \textbf{(3-2)}$$

The implied condition (seldomly made explicit) for above equations is that the antenna thickness has to be impractically small.

Later, it is shown that even a slight change in antenna dimension leads to a considerable change in impedance. Therefore, whether this considerable change can be reproduced becomes a test criteria for software packages. Each simulation software package has its range of dipole dimensions (length, diameter) where we can be confident of the accuracy. Our goal is to find the ranges so that we can be confident in the results for different dipole configurations.

2.3 Impedance Results

The model used in the verification is the elementary dipole antenna, as demonstrated in Figure 2.1.

Unless otherwise specified, the wavelength (λ) used in this chapter is 300mm, corresponding to 1GHz. The total length of the dipole antenna is 0.5λ, and the gap size is 2mm. For a perfect conductor, the results will be independent of frequency. But if a real-world conductor, such as copper, stainless steel, etc., is used, then the antenna will have losses, and the impedance will include the impact of the losses. For copper, there is little change (loss) until the frequency reaches several tens of GHz.

Figure 2-1 Demonstration of a Straight Dipole Model

2.3.1 Simulation Approaches

The simulation approaches are categorized into two groups. One is the antenna with a very small (impracticable) radius, and the other is the antenna with a larger (practical) radius.

2.3.1.1 Small Radius Verification

Previously, we mentioned that CST cannot provide an accurate solution if the range of dimensions (width and length) is very small. This is due to its sensitivity to the calculations over small mesh grids, so the CST has been excluded from the evaluation.

The radius has been assigned to have a range from 0.00001λ to 0.01λ, as shown in Table A.

TABLE A Radius of the dipole antenna in simulation (Small)

Radius in λ	***Radius in (mm)***
$1X10^{-5}$	0.003mm
$5X10^{-5}$	0.015mm
$1X10^{-4}$	0.03mm
$5X10^{-4}$	0.15mm
$1X10^{-3}$	0.3mm
$5X10^{-3}$	1.5mm
$1X10^{-2}$	3mm

The theoretical dipole impedance of $73+ j42\Omega$ is expected when the radius is very small. HFSS and WIPL-D are used in this comparison. The results for both the real part and the imaginary part are shown in Figure 2.2.

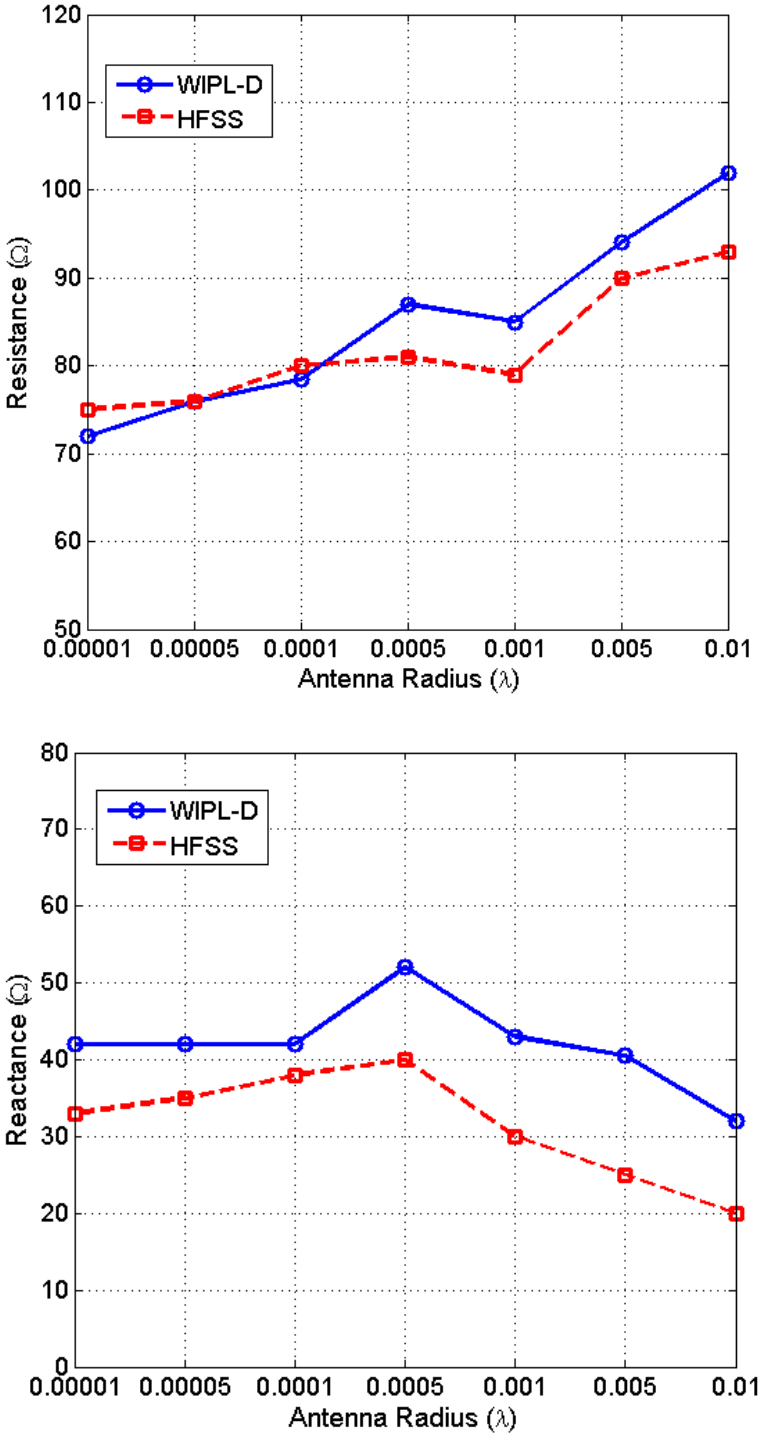

Figure 2-2 HFSS and WIPL-D simulated impedance in small radius

In this configuration, both HFSS and WIPL-D are accurate for the resistance. They are close to the theoretical result when the radius is quite small. For the imaginary part, only WILP-D yields a theoretical reactance of 42Ω.

However, due to the segmentation structure limitation of Method of Moments employed by WIPL-D (the wire segment lengths must be much longer than their widths), it is not expected to provide an accurate value when dipole radius becomes large. (See Section 2.3.1.2 Large Radius Verification)

2.3.1.2 Large Radius Verification

The second group uses a large radius, ranging from 0.01λ to 0.05λ, as shown in Table B.

Since the model dimension becomes large enough, CST can provide a valid solution. WIPL-D, although not expected to simulate an accurate result, is still evaluated as a reference. The results are illustrated in Figure 2.3.

TABLE B Radius of the dipole antenna in simulation (Large)

Radius in λ	***Radius in (mm)***
$1X10^{-2}$	3mm
$2X10^{-2}$	6mm
$3X10^{-2}$	9mm
$4X10^{-2}$	12mm
$5X10^{-2}$	15mm
$6X10^{-2}$	18mm

For the resistance part, the HFSS and CST begin to get closer to each other when the radius becomes larger, even overlapped at the last several points. This is because the fundamental methods used by these two packages share some similarities. On the other hand, the WIPL-D results disagree with those of HFSS and CST. For the reactance part, although HFSS and WIPL-D are close at the first several points, when the radius becomes larger, CST and HFSS demonstrate the same trend.

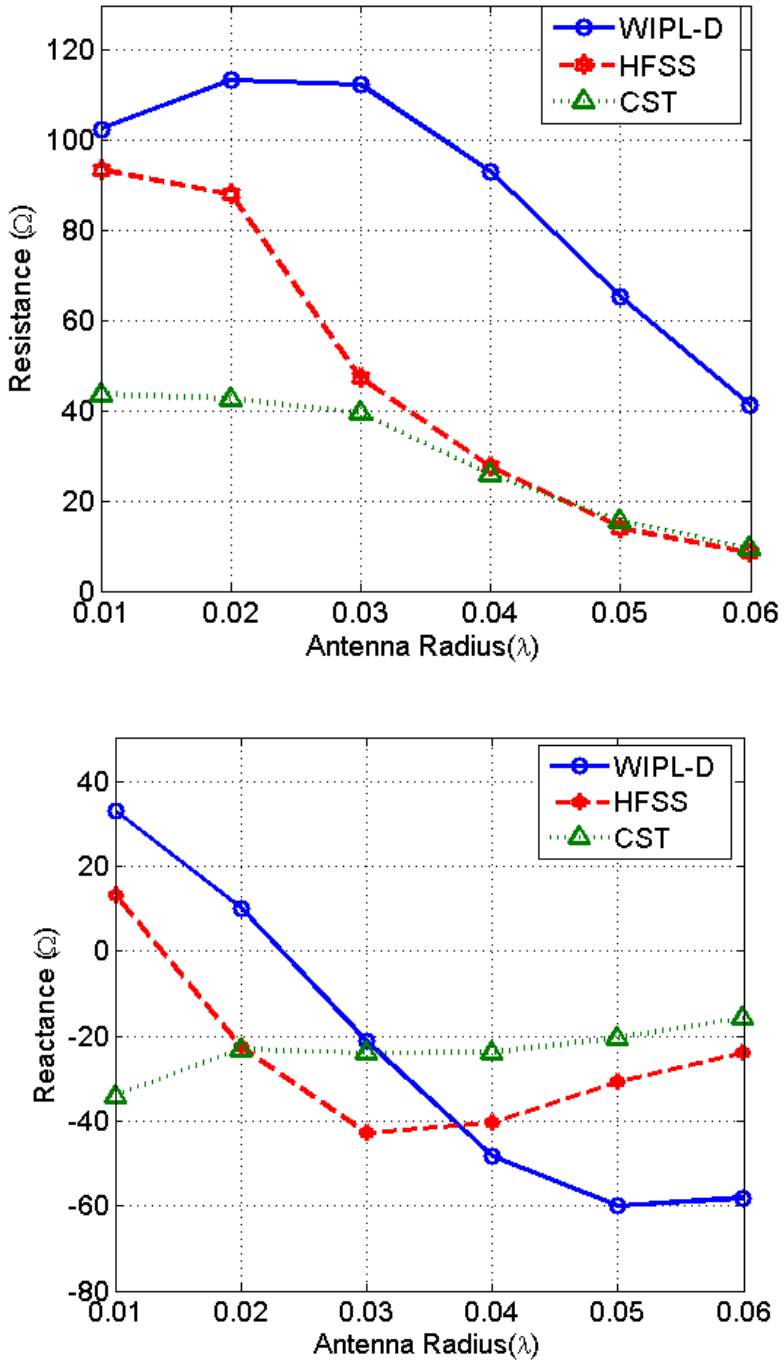

Figure 2-3 HFSS, CST and WIPL-D simulated impedance in practical radius

2.3.2 Analytical Approaches

The simulated results have been presented in the above section. In this section, two analytical methods are used to calculate the dipole impedance, the Wave-Structure Method and Induced EMF Method.

2.3.2.1 Wave-Structure Method

A theoretical approach for treating the dipole impedance is the Wave-Structure method [13]. The method is based on space-surface wave structure approach derived by Andersen in the 1960s and later by Jones in the 1980s (see [13]).

According to this method, the dipole impedance relies on the electrical length and radius of the dipole. The derivation of this method is not discussed here, but the general results are given below.

For a lossless, thin monopole antenna of length $L_{monopole}$ (the equivalent dipole has a total length $L_{dipole}=2L_{monopole}$), the input admittance is

$$Y_{monopole} = \frac{-2\pi}{z_0 \log(\frac{ka_{monopole}\,\Gamma}{2})} + \frac{4\pi}{z_0 \log(\frac{a_{monopole}}{2L_{monopole}})e^{j2kL_{monopole}} + 1 + \frac{\log(j4kL_{monopole}\,\Gamma)}{2\log(ka_{monopole})}} \quad \textbf{(2-3)}$$

where the $Z_0 = 120\pi$ is the free space impedance, $a_{monopole}$ is the antenna radius, $k = \frac{2\pi}{\lambda}$ is the wave number, and $\Gamma = e^{\gamma} = 1.781$, in which γ is the Euler constant=0.5772.

Therefore, the resistance $R_{monopole}$ and reactance $X_{monopole}$ can be obtained using the admittance $Y_{monopole}$, illustrated in Figure 2.4.

Figure 2.4 shows that the Wave-Structure Method behaves differently from the simulated results under a practical radius ($\alpha_{monopole}$=0.01λ). This is mainly because the Wave-Structure Method seems to break down for wires with a larger radius.

Another group of simulations was performed using an extremely small antenna radius ($a_{monopole}$=1×10^{-7}λ). The results obtained from the Wave-Structure method are closer to the simulated results for this configuration. However, the difference is still significant. The impedance results are illustrated in Figure 2.5.

Another comparison for the Wave-Structure method against the measured results can be found in Section 2.3.3.

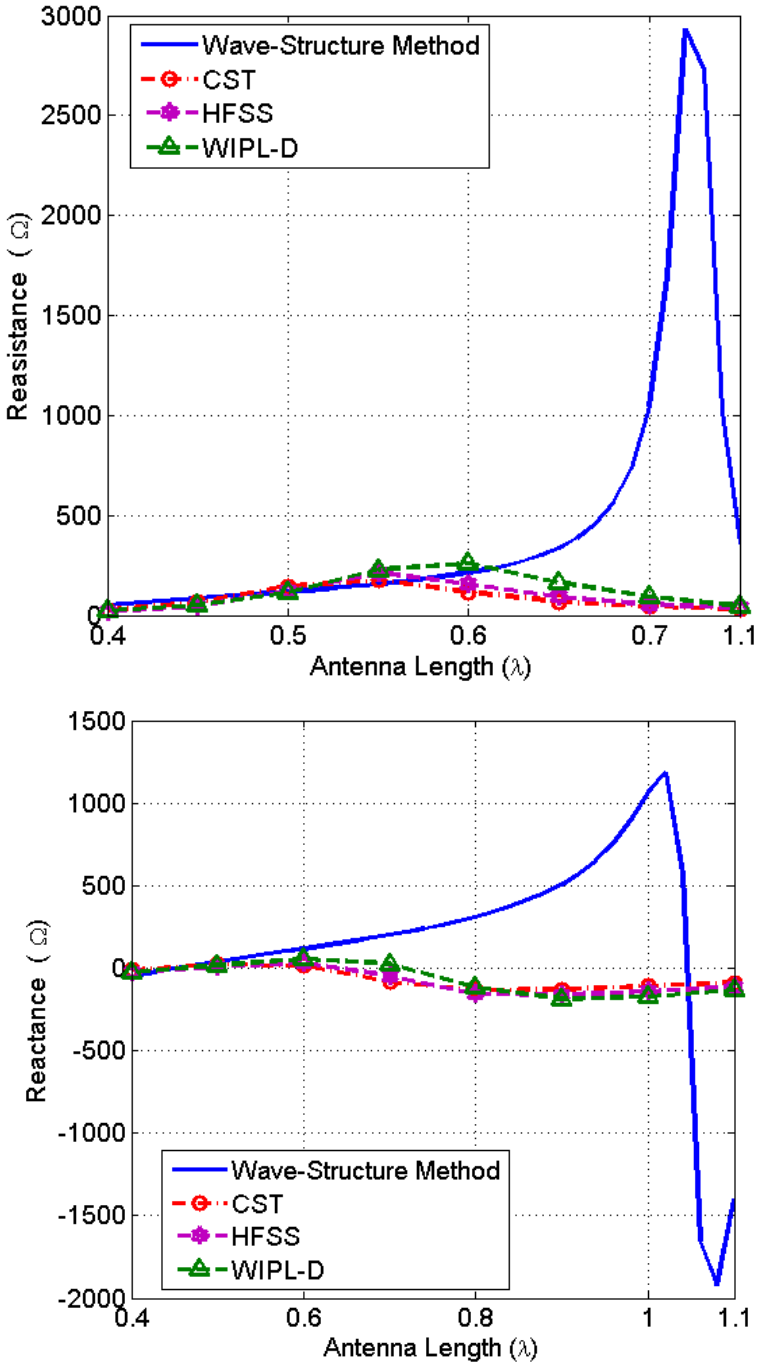

Figure 2-4 Impedance results of Wave-Structure Method under practical radius ($\alpha_{monopole}$=0.01λ)

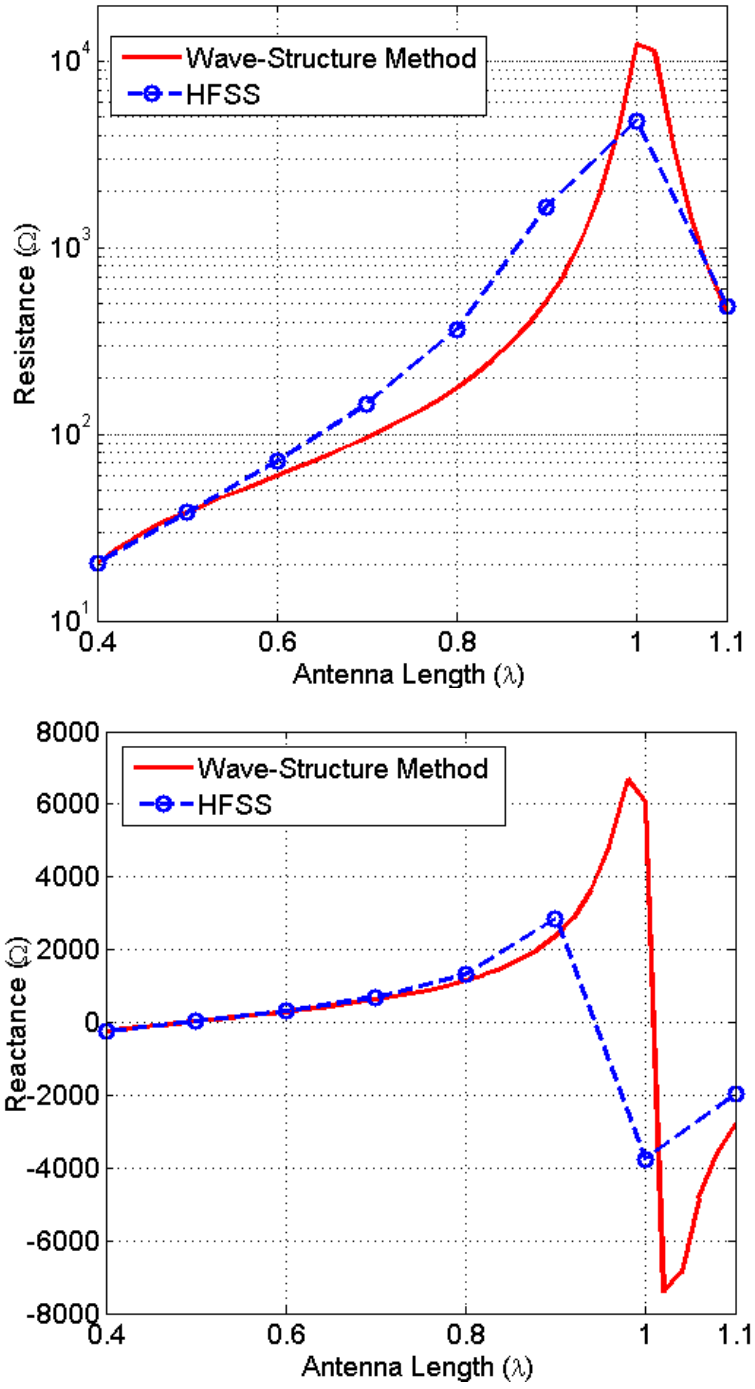

Figure 2-5 Impedance results of Wave-Structure Method under extremely small radius

($a_{monopole}$=1×10^{-7}λ)

2.3.2.2 Induced EMF Method

The induced EMF Method was originally introduced by L.Brillouin in 1922 (see [13]). The following well known equations can be deduced from [13]

$$Z_{molopole} = \frac{V}{I_{max}}\left(-\frac{1}{I_{max}}\int_{-\frac{L}{2}}^{\frac{L}{2}} E_z\left(a_{monopole}, z'\right) I_Z\left(a_{monopole}, z'\right) dz'\right) =$$
$$-\frac{1}{I_{max}}\int_{-\frac{L}{2}}^{\frac{L}{2}} E_z\left(a_{monopole}, z'\right) sin\left(k\left(\frac{L}{2} - \left|z'\right|\right)\right) dz' = R_{monopole} + jX_{monopole}$$

(2-4)

The resistance is

$$R_{monopole} = \frac{Z_0}{2\pi}(\gamma + ln\left(kL_{monopole}\right) - Ci\left(kL_{monopole}\right) + \frac{1}{2} sin\left(kL_{monopole}\right) S_1$$
$$+ \frac{1}{2} cos\left(kL_{monopole}\right) C_1)$$

(2-5)

And the reactance is

$$X_{monopole} = \frac{1}{sin^2 kL_{monopole}} \frac{Z_0}{4\pi}(2Si\left(kL_{monopole}\right) - cos\left(kL_{monopole}\right) S_1$$
$$- sin\left(kL_{monopole}\right) C_2)$$

(2-6)

where

$$S_1 = Si(2kL) - 2Si(kL) \quad \textbf{(2-7)}$$

$$C_1 = \gamma + ln\left(\frac{kL}{2}\right) + Ci(2kL) - 2Ci(kL) \quad \textbf{(2-8)}$$

$$C_2 = 2Ci(kL) - Ci(2kL) - Ci(\frac{2ka^2}{L}) \quad \textbf{(2-9)}$$

Only the reactance, $X_{monopole}$, relies on the dipole radius (a), and this dependence will drop out if the length is a multiple of half-wavelength. Therefore, the entire equation above shows the resistance is independent of the radius, and the reactance becomes periodic with the change of the antenna length.

2.3.3 Measured Results

The simulation and analytical results are given in above sections. However, since the inconsistency still exists, we cannot tell which one actually provides a trustworthy result. Therefore, some physical measurement results have been employed to confirm the accuracy of the simulation [25] - [28]. One of them is from Mack's measurement [25] and another is our measurement using a Vector Network Analyzer (VNA).

2.3.3.1 Mack's Results

Mack's measurement used a dipole antenna with a radius of 0.007022 wavelengths.

A similar scenario has been duplicated in our simulation packages. The antenna dimension in the software matches Mack's. The material is set to be copper although the material is not mentioned in the description of Mack's measurements [25].

The comparison of Mack's measured results with our simulated and analytical results is in Figure 2.6.

This comparison clearly demonstrates the Wave Structure Method is not accurate even for moderately small dipole radii. It will only be useful when the radius of the structure is less than 1×10^{-7} of the wavelength.

For the simulation packages, both WIPL-D and HFSS provide similar results to the measurements. For the reactance, all three almost coincide at some points, which is a surprising result.

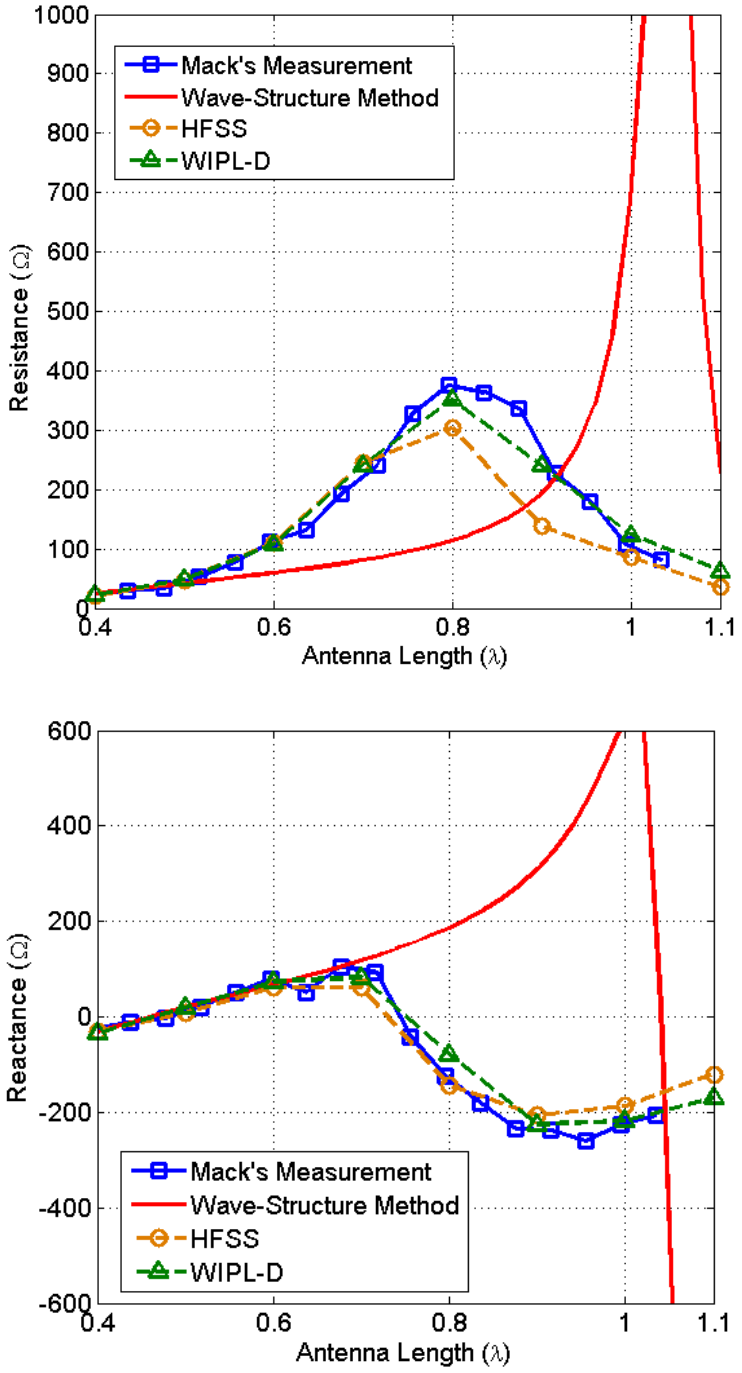

Figure 2-6 Mack's measurement results compared with Wave-Structure Method, WIPL-D and HFSS results

2.3.3.2 Measurement of dipole antenna in different length

Another group of physical experimental results is obtained using an Agilent VNA. Monopole antennas with different lengths was built, and then measured using the VNA. The set-up is shown in Figure 2.7.

Figure 2.8 demonstrates that the physical measurements match the simulations, although the measurement result maybe higher at certain lengths. Considering that the measured antenna is made from lossy material and the testing environment is not perfect, the difference observed is not too surprising.

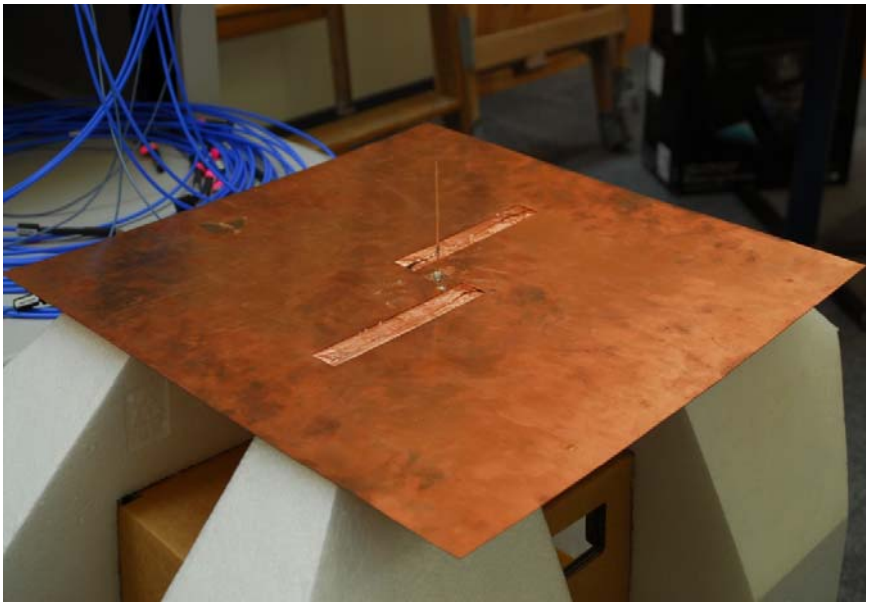

Figure 2-7 Demonstration of measured monopole antenna

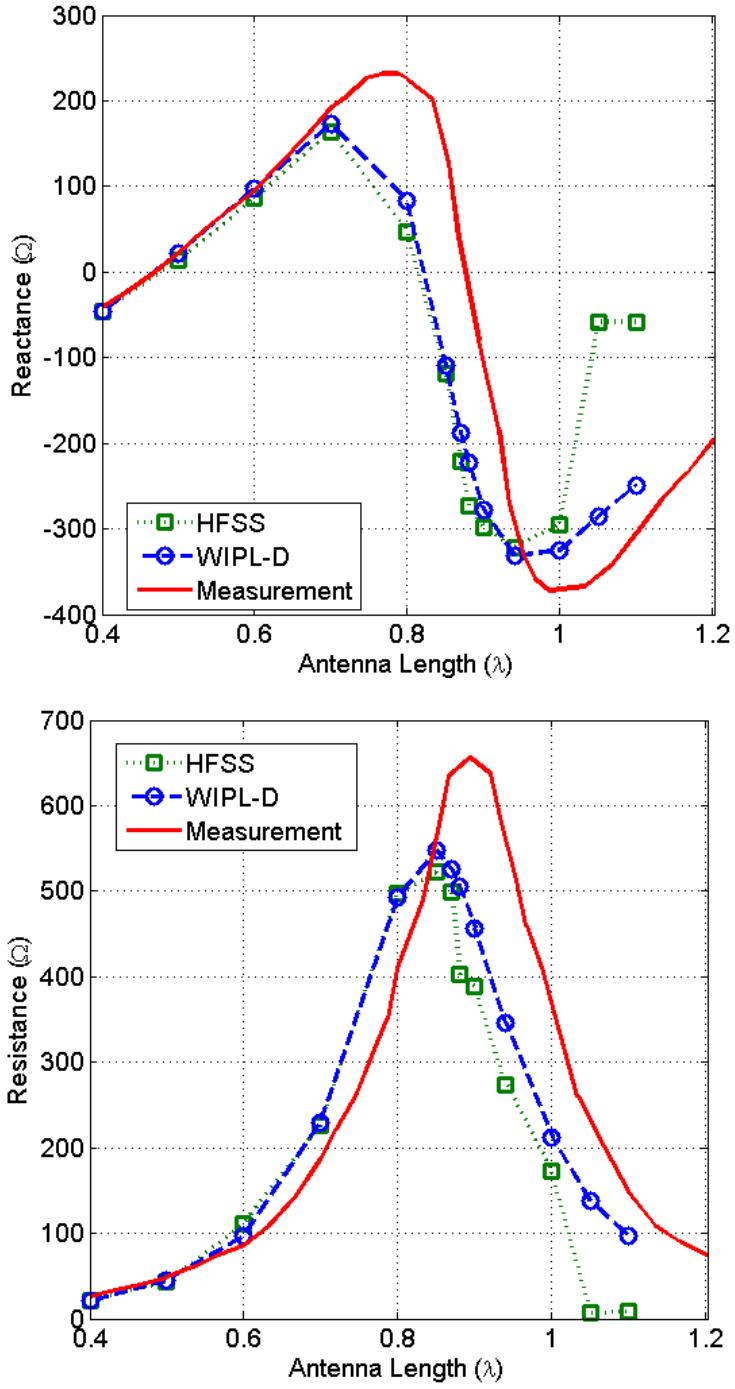

Figure 2-8 Measurement results compared with HFSS and WIPL-D simulation results

2.4 Summary

In this chapter, we focused on the impedance accuracy of different simulation software packages. Since there are no theoretical impedance results of a dipole antenna with practical dimensions, some impracticable (i.e., too thin to be robust) dimensions are discussed, which have analytical results. Through a verification process for an elementary dipole antenna, the advantages and limitations of each simulation package can be determined.

WIPL-D utilizes the Method of Moments. This provides an excellent match with the theoretical results when the antenna radius is very small. However, for the simulations of antenna with a thicker, more practical radius used in reconfigurable antenna application, WIPL-D is not expected to yield an accurate result since the assumption of thin wires of the Method of Moments is not satisfied.

CST is one of the most popular microwave simulation packages. Generally speaking, CST is suitable for models with a lower range of dimensions. However, since it is sensitive to small mesh grid settings, we only use CST as a backup simulator for the reconfigurable antenna application.

HFSS is the most powerful software package and can provide accurate results for various antenna dimensions. Therefore, we choose HFSS as the principal simulator for the diversity analysis of the reconfigurable antenna.

3: RECONFIGURABLE ANTENNA APPLICATION (WIRE PARASITIC ELEMENT)

In this chapter, a new idea for a reconfigurable antenna is proposed, which employs two moveable parasitic elements around a fixed monopole antenna. Some characteristics have already been discussed in Chapter 1. The principal objective is to achieve diversity performance as well as the pattern-changing ability.

One of the most important advantages of this reconfigurable antenna is that the active RF element is stationary. (Strictly speaking, the parasitic elements also bear RF currents, but there are no active RF devices attached to these, as in many switched parasitic configurations.) The only moving part is the parasitic element, which reduces the complexity of a mechanically moving system.

The parasitic elements in the proposed model are simple metal wires, namely V-Shaped parasitic elements. This particular shape of parasitic element is a more simple solution to alter the radiation pattern than any other wire

parasitic configurations. Some of other configurations and their results, are presented in a later section of this chapter.

In this thesis, only the electromagnetic side of the antenna is discussed. The mechanical technique used to move the parasitic elements is demonstrated in [28]. This technique utilizes electro active polymers to drive the parasitic elements. However, owing to the limited weight that can be handled, the parasitic elements are implemented with light metal wires. Chapter 5 will introduce another solution with parasitic elements - composed of heavier metal sheets.

This chapter has the following sections. Section 3.1 provides the demonstration of the modelled antenna, and the important parameters are defined in this section. Section 3.2 characterizes how much the pattern is changed. Section 3.3 provides a comprehensive parametric study and the diversity results. Other different shapes of wire parasitic elements, and their performance, are introduced in Section 3.4. Finally, Section 3.5 summarizes the work within this chapter.

3.1 Demonstration of the Proposed Model

The proposed model in this chapter is a monopole antenna on a groundplane with two V-Shaped parasitic elements beside it, in opposing orientation. The parasitic elements counter-rotate around a common axis. Detailed movements are illustrated in Figure 3.1 and Figure 3.2.

In these figures, the rotating angle α is the basic angle which measures how far the parasitic elements are rotated. This is a fundamental parameter used in the simulation to produce the pattern-changing effect and the associated diversity performance. Figure 3.1 shows the antenna in its original position with a rotating angle $\alpha=0^{o}$, and Figure 3.2 shows the model when the rotating angle $\alpha=60^{o}$.

The wavelength is set to be 300mm in the simulation. The antenna is working at the frequency of 1GHz. The following dimensions are fixed as a ratio of wavelength.

- Active element (monopole antenna) length: 1/4 λ (75mm)
- Active element radius: 0.003λ (1mm)
- Parasitic elements radius 0.003λ (1mm)

The following variables are partially optimized (by simulation software) in the simulation since they impact the diversity performance.

- Bend angle: β_v
- Total length of one V-Shaped parasitic element: L_v
- Groundplane length: R
- Distance between antenna and parasitic elements: d

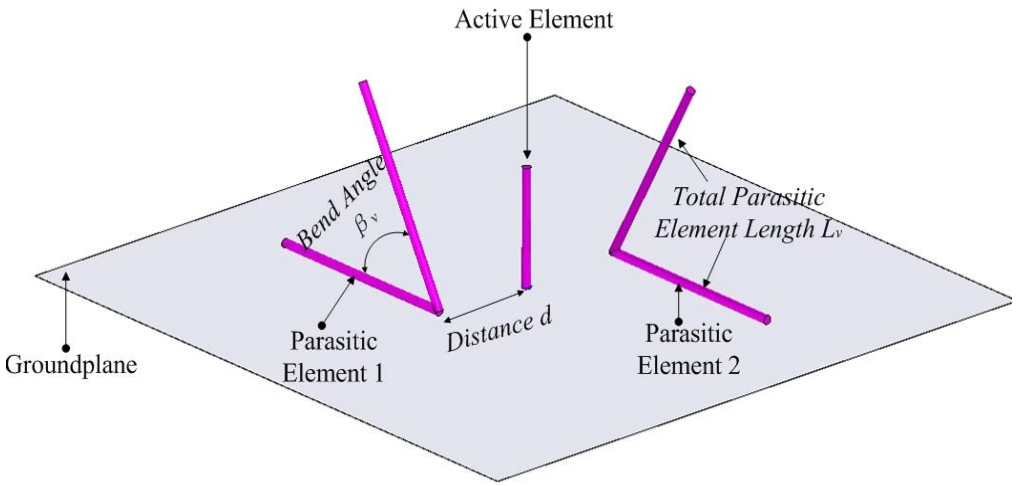

Figure 3-1 Configuration of the proposed model with parasitic elements in their original position (i.e. rotating angle α equals to 0^o)

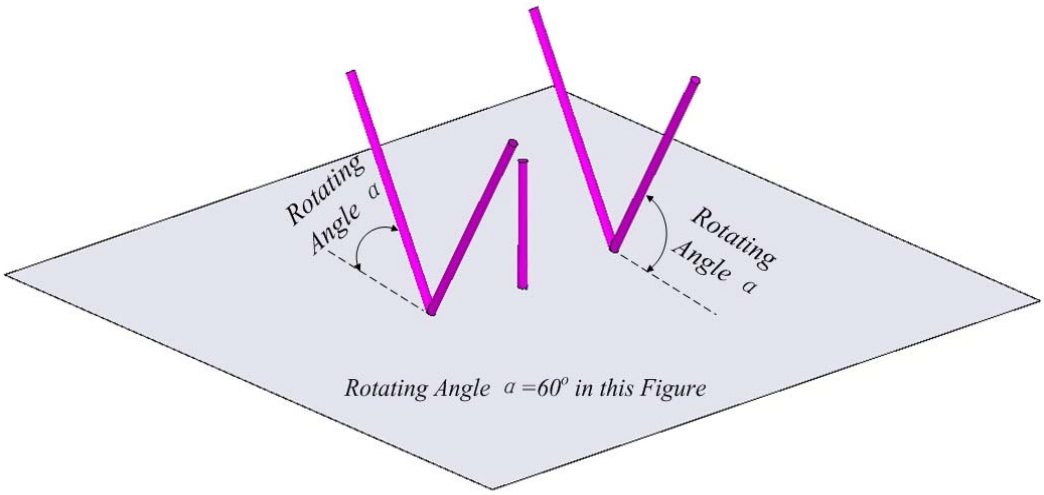

Figure 3-2 Configuration of the proposed model with parasitic elements moved 60° (i.e. rotating angle *α* equals to 60°)

3.2 Far-field Pattern Change

HFSS is used to simulate antenna radiation pattern and impedance, since the accuracy of this particular software has already been verified. Figure 3.3 shows the antenna gain pattern (power pattern, i.e., both polarizations) in a horizontal cut (θ=90°). The maximum gain in this cut is 5.2dBi, and the gain can be higher for other directions or other rotating angles. This is because the parasitic elements and the finite groundplane – particularly diffraction from the

edges – contribute to the radiation. The two rotating angles demonstrated in this figure are 0^o and 60^o, which are the positions shown in Figure 3.1 and 3.2.

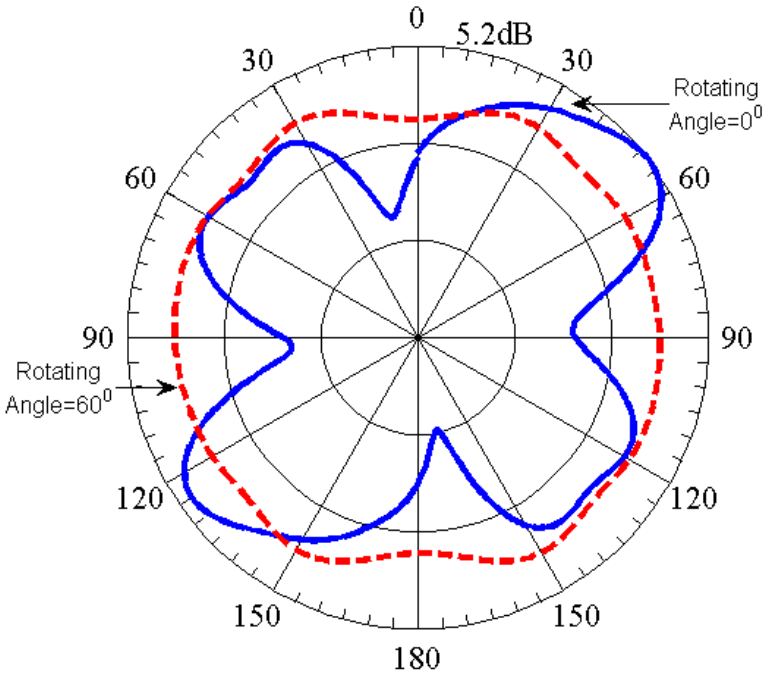

Figure 3-3 Antenna Directive Gain in dB at different rotating angles

An obvious change in the radiation pattern can be observed from the figure, and this type of change can be found in all other rotating angles as well. Therefore, the objective of changing the pattern is accomplished.

Furthermore, since the far-field pattern has been significantly changed, good diversity action can be expected (see [13]). Section 3.3 defines the

correlation term used in this chapter, and Section 3.4 demonstrates the achieved diversity in terms of the correlation coefficient.

3.3 Diversity Performance

Correlation is a value used to evaluate the diversity, and the correlation mentioned in the thesis is the far field pattern correlation. Much work has been undertaken in [13] to provide diversity results.

The correlation coefficient is the normalized correlation with a maximum value of 1, which means the two patterns are identical, i.e., fully correlated. The definition of the normalized autocorrelation coefficient is

$$\rho = \int_0^{2\pi} \int_0^{\pi} S(\theta, \varphi) |E(\theta, \varphi)|^2 sin\theta d\theta d\varphi = 1 \quad \textbf{(3-1)}$$

In (3-1), $S(\theta,\varphi)$ is the probability density function (pdf) of incident waves at the antenna, referred to antenna coordinate. For an omnidirectional antenna case such as dipole antenna used in the thesis, the $S(\theta,\varphi)$ is generally considered as 1. The $E(\theta,\varphi)$ is the normalized far-field pattern of an antenna expressed as a vector for both (θ and φ) polarizations.

The definition of the correlation coefficient between two patterns is

$$\rho_{12} = \int_0^{2\pi} \int_0^{\pi} S(\theta,\varphi) E_1(\theta,\varphi) \cdot E_2^*(\theta,\varphi) sin\theta d\theta d\varphi \quad \textbf{(3-2)}$$

$E_1(\theta,\varphi)$ and $E_2(\theta,\varphi)$ are the two far-field patterns. Ideally the correlation coefficient equals 0 which means two antenna patterns are uncorrelated or orthogonal. However, such a result is very difficult to achieve in a limited space. Diversity can be effective if the correlation coefficient is below 0.7 [13]. The results from later sections confirm that the reconfigurable antenna can achieve a much lower correlation coefficient.

The far-field pattern, simulated from the antenna in its original position (i.e. rotating angle $\alpha=0$) is defined as $E_1(\theta,\varphi)$, is in Figure 3.1. The $E_2(\theta,\varphi)$ is the far-field pattern in second position (the parasitic elements of the antenna are rotated by α). The correlation coefficient between $E_1(\theta,\varphi)$ and $E_2(\theta,\varphi)$ would be ρ_{12}, demonstrated in (3-2). This correlation is based on uniform, uncorrelated, incident waves in both θ and φ polarizations, over the hemisphere above the groundplane.

Several parameters list in Section 3.1 could produce the change in the far-field pattern hence the correlation. Under certain configurations, the correlation

coefficient can drop as low as about 0.1. This result satisfies requirements for a good diversity.

However, since the parasitic elements are close to the active element, the impedance matching is affected. Therefore, a parametric study is performed in order to achieve a low correlation coefficient and still maintain an impedance match when the parasitic elements rotate.

3.3.1 Bend Angle

The bend angle β_v is the angle separating the two wire arms of V-Shaped parasitic element. It restricts the upper bound of the rotating angle since the V-Shaped parasitic element has to remain above the groundplane, e.g. V-shaped parasitic elements with bend angle at 60^o can only rotate 120^o before they touch the other side of the groundplane. Therefore, smaller bend angle means larger rotating range.

The following bend angles have been simulated, $\beta_v = 30^o, 45^o, 60^o, 75^o, 90^o$.

Figure 3.4 shows the correlation coefficient results between the antenna pattern at the original position (i.e. rotating angle α equals to 0^0) and the pattern

of the antenna in other positions where the parasitic elements have been rotated by α (illustrated in x-axis). Different curve colours (and markers) represent different bend angle, β_v, used by the parasitic elements. The correlation coefficient in the figure is $|\rho_{12}|$ in (3-2). The envelope correlation coefficient, $|\rho_{12}|^2$, is even lower.

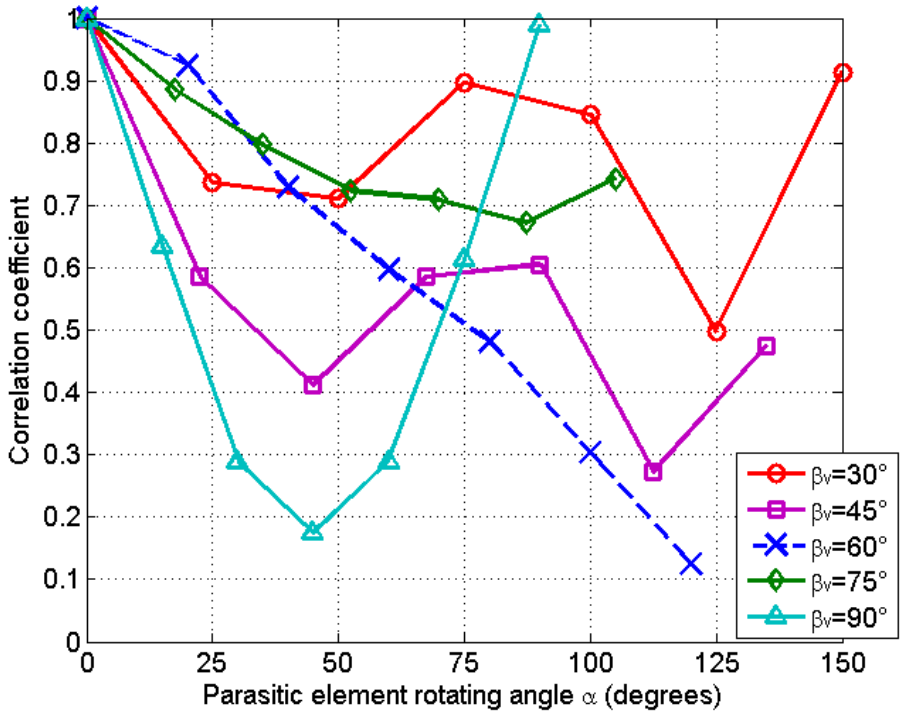

Figure 3-4 Pattern correlation coefficient of the antenna under different bend angles

The correlation curve of the antenna with the bend angle β_v at 90^o, shows good diversity (has a quickly-dropping correlation coefficient function) with

minimal parasitic elements rotation (correlation coefficient curve drops fastest when the parasitic elements are rotated 45^{o}). But it has a higher correlation coefficient for larger rotating angles. This is because the model has a symmetric design at the beginning and ending positions, making the active elements parallel with one arm of each parasitic element. Considering the antenna has a relatively small rotating range, the bend angle at 90^{o} is not recommended.

The antenna configuration with the bend angle β_V=45^{o}, although also achieving a low correlation coefficient of approximately 0.28, provides an non-monotonic correlation curve.

On the other hand, the antenna with the bend angle at 60^{o} reaches the lowest correlation at 0.1 and provides a steady and monotonically decreasing correlation curve.

Figure 3.5 shows the resistance of the active element against the rotating angles for different bend angles. The antenna with different bend angles can provide a relatively stable curve except for the bend angles β_V=30^{o} and 45^{o}. Therefore, considering the correlation results obtained so far, 60^{o} seems a good option for the bend angle.

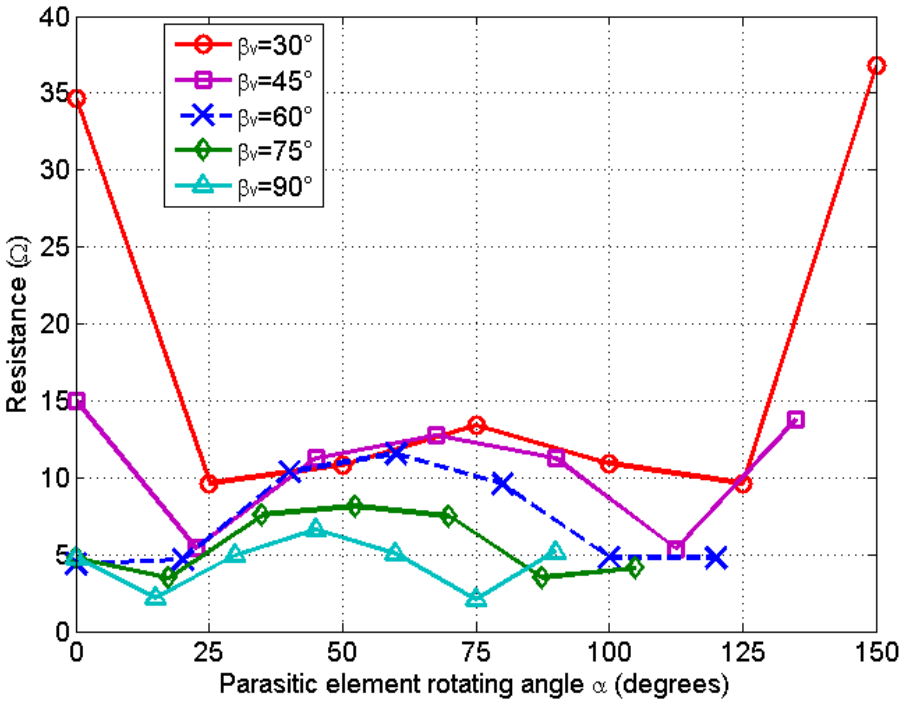

Figure 3-5 Resistance of the antenna under different bend angles

3.3.2 Distance between active and parasitic elements

The distance between the active element and the parasitic elements, *d,* is another significant parameter, since both correlation and impedance are very sensitive to such distance. If the distance is too large, the far-field pattern will not be strongly impacted by the parasitic elements.

For the bend angle set to be 60°, the following distances have been simulated:

d=0.05λ, 0.1λ, 0.2λ, 0.3λ, 0.5λ.

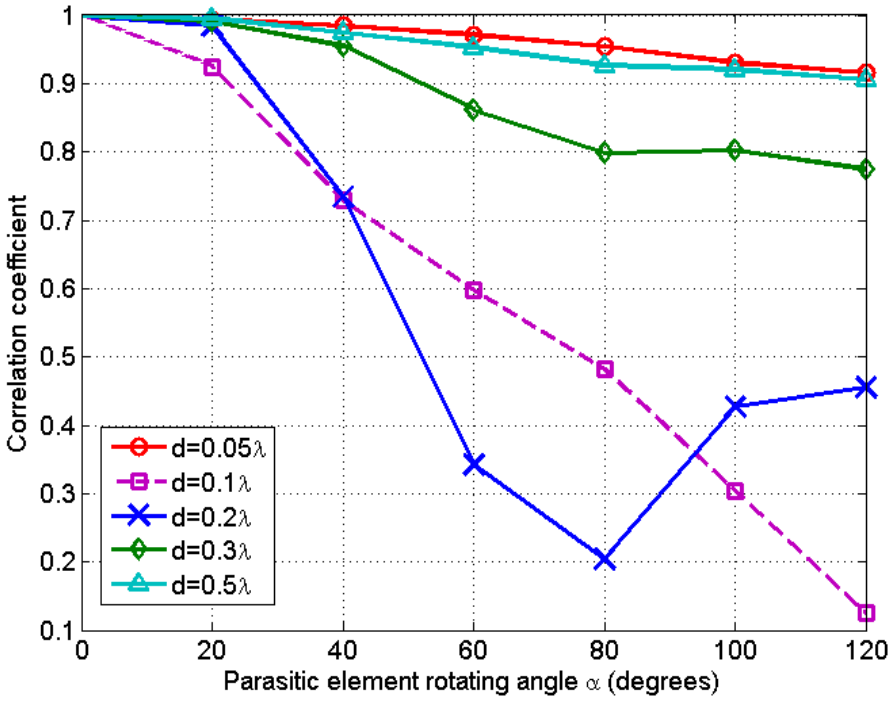

Figure 3-6 Pattern correlation coefficient of the antenna under different distances between active and parasitic elements

It clearly shows that the parasitic elements with distances larger than 0.2λ from the active element will not bring much pattern-changing effect. The antenna with a separation distance of 0.05λ yields an even flatter correlation curve, meaning that the parasitic elements have a minimum interference in the far-field

pattern. Therefore, only distances at 0.1λ and 0.2λ can bring enough reduction of the correlation.

Given the consideration of the impedance matching demonstrated in Figure 3.7, the distance between antenna and parasitic elements should be between 0.1λ and 0.2λ.

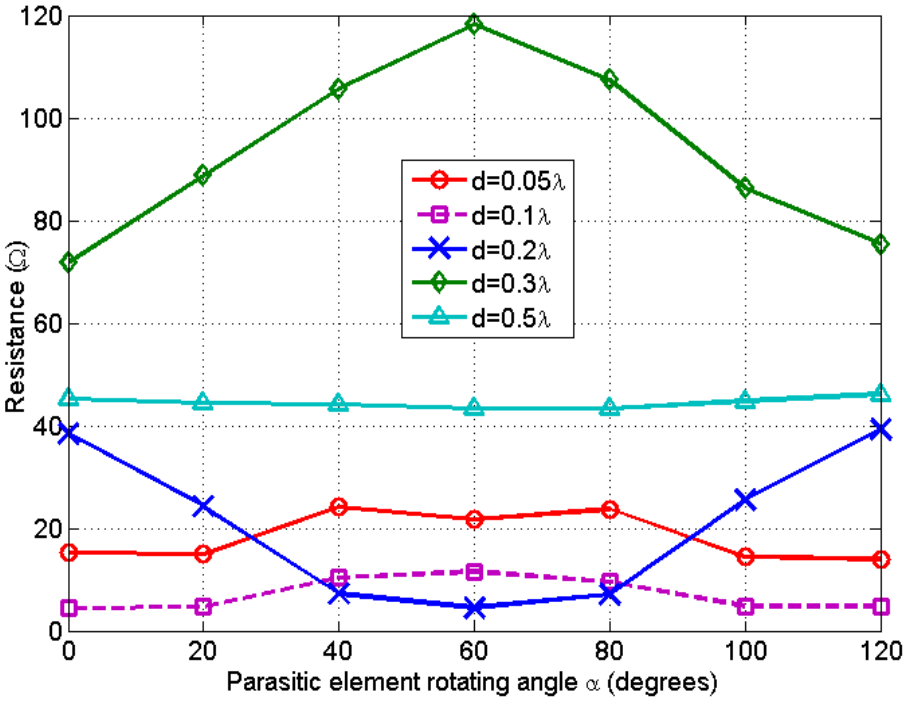

Figure 3-7 Resistance of the antenna under different distances between active and parasitic elements

3.3.3 Length of the parasitic elements

The length of the parasitic L_v is defined as the total length of a single V-Shaped parasitic element, including both wire arms. This length must be sufficient to affect the correlation coefficient.

The bend angle is set at 60^o with the distance between antenna and parasitic elements set at 0.1λ. The following parasitic element lengths have been simulated: *L_v=0.75λ, 1λ, 1.25λ, 1.5λ.*

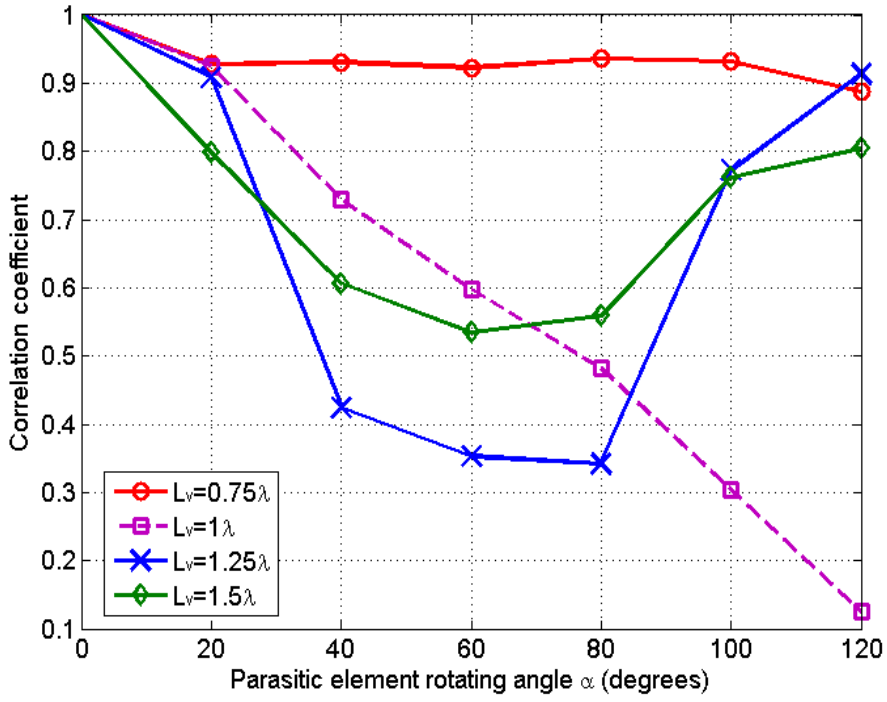

Figure 3-8 Pattern Correlation coefficient of the antenna under different length of the parasitic elements

Figure 3.8 shows the correlation of the original antenna pattern against the antenna pattern with the rotation of the parasitic elements for different parasitic element lengths. The results confirm that lengths smaller than 0.75λ lead to an 'invisible dipole' phenomenon [13]. Here, any parasitic element beside the active element will not affect the antenna performance, because they are electromagnetically invisible, often referred to as a minimum scattering antenna. However, antenna with longer parasitic elements of 1.25λ or 1.5λ has no better diversity performance than the antenna with parasitic elements *at 1λ*.

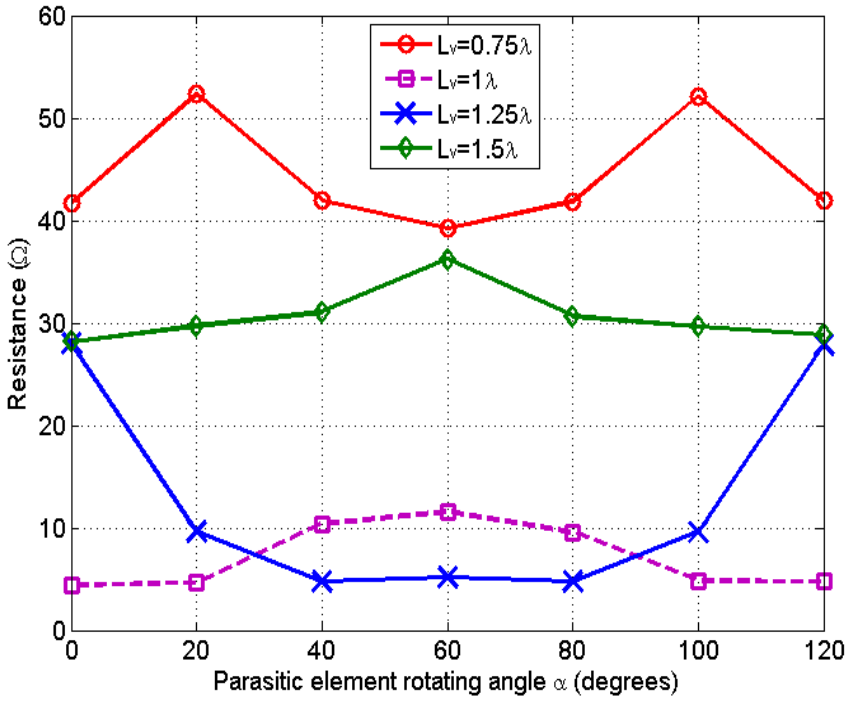

Figure 3-9 Resistance of the antenna under different length of the parasitic elements

3.3.4 Groundplane length

The groundplane used in this model is a square. Other shapes of groundplane can also be used. Simulation results demonstrated that the impact on correlation performance for different groundplane sizes is minimal if the groundplane length is larger than 1.5λ.

The length of the parasitic elements is set to be 1λ according to previous simulations. The following groundplane lengths have been simulated:

R= 0.5λ, 1λ, 1.5λ, 2λ, 3λ.

Figure 3.10 shows the correlation results between the antenna with parasitic elements at the original position and at other positions. Almost no difference can be identified in the correlation curves if the groundplane is larger than 1.5λ. The antenna with a groundplane size as small as 0.5λ has a strongly decreased diversity performance.

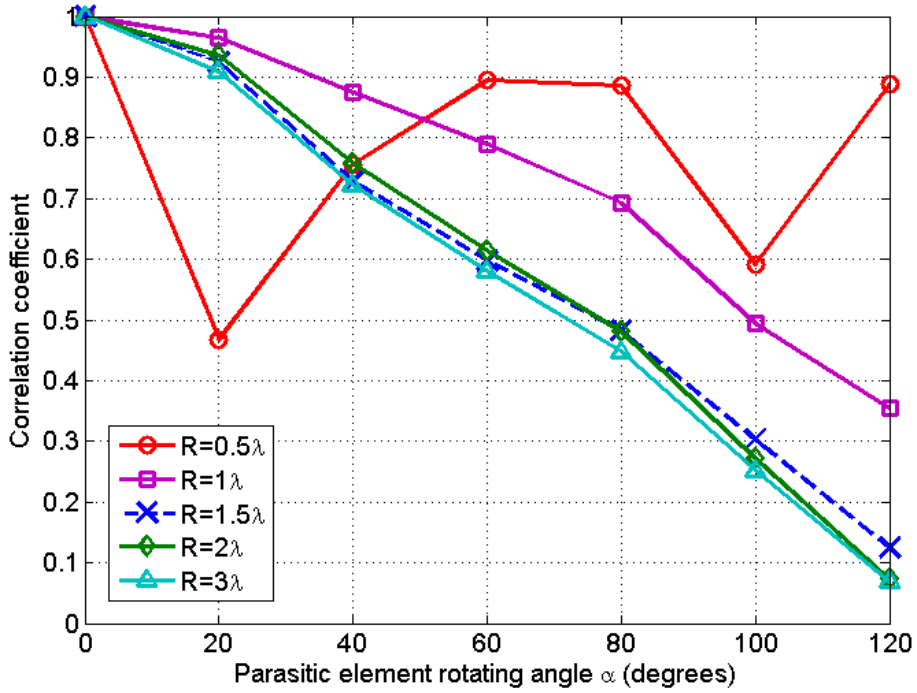

Figure 3-10 Pattern correlation coefficient of antenna under different groundplane length

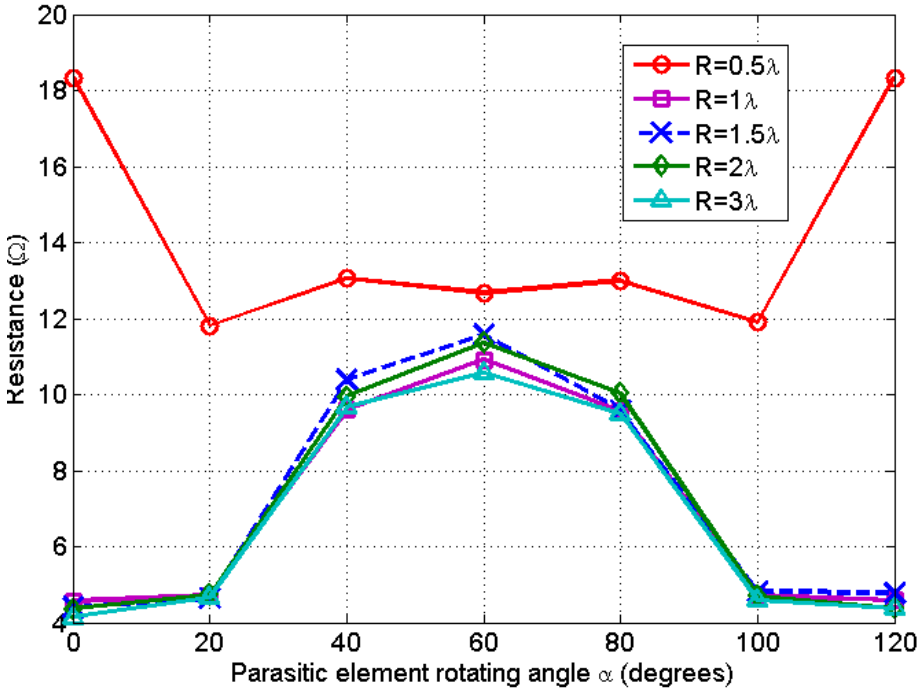

Figure 3-11 Resistance of the antenna under different groundplane lengths

Figure 3.11 demonstrates the resistance of the antenna with the rotating of parasitic elements using different groundplane lengths. As expected, minimal difference can be observed when the groundplane length is larger than 1λ. Based on the correlation results obtained before, the groundplane length should be 1.5λ.

3.3.5 Recommended value of each parameter

Finally, the recommend ranges of the parameters have all been collected in Table C.

TABLE C Recommended parameter values for the reconfigurable antenna with wire parasitic elements

Symbol	***Definition***	***Value***
β_v	Bend Angle	45^o -60^o
D	Distance between antenna and parasitic elements	0.1λ-0.2λ
L_v	Length of the parasitic elements	1λ
R	Groundplane length	≥1.5λ

3.4 Other Examples

Both pattern and correlation results for the model with two parasitic elements have been introduced. Some other shapes of parasitic elements are also evaluated.

3.4.1 Single parasitic element

In this model, one of V-Shaped parasitic elements has been completely removed, as demonstrated in Figure 3.12. All the parameters are choosn according to the antenna with dual parasitic elements

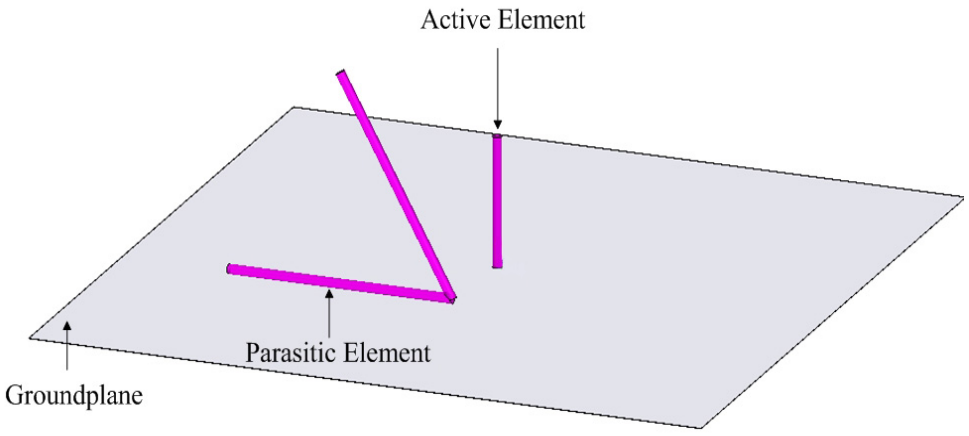

Figure 3-12 Demonstration of the antenna with single parasitic element

The values of the important parameters is chosen according to Table C.

Figure 3.13 demonstrates the pattern correlation of the antenna with the parasitic element is at the original position and with the parasitric oriented at all other positions. The decrease of the correlation curve is similar between those two antenna models. However, the lowest correlation coefficient for the antenna with single parasitic element only reaches about 0.4.

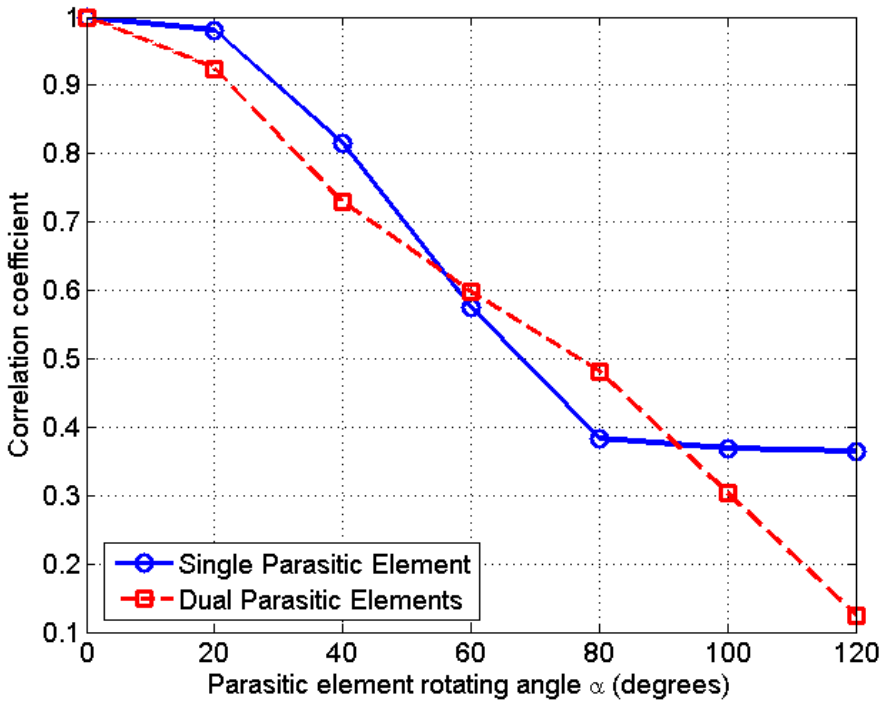

Figure 3-13 Pattern correlation coefficient of the antenna with single parasitic element and dual parasitic elements

Figure 3.14 shows the antenna impedance under different rotating angles for both models. The antenna with a single parasitic element has a varying impedance curve. Moreover, since one of the parasitic elements is removed, the pattern-changing ability is reduced.

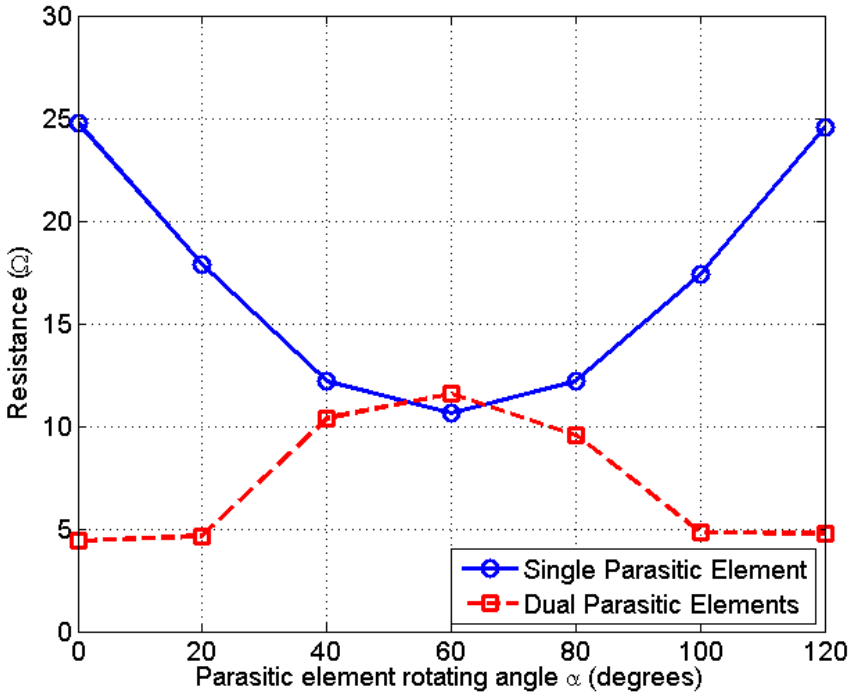

Figure 3-14 Resistance of the antenna with single parasitic element and dual parasitic elements

It can be concluded that the antenna with single parasitic element has almost same diversity performance in most scenarios. Therefore, both models

are suitable for array applications, although we use the dual parasitic elements model in this thesis for achieving maximal diversity performance. If the model complexity is a concern or the pattern-changing ability is considered less important, then the single parasitic element model is a good choice.

3.4.2 Trident Model

The Trident-Shaped parasitic element comprises three wire arms instead of the two in the proposed model. The model is depicted in Figure 3.15.

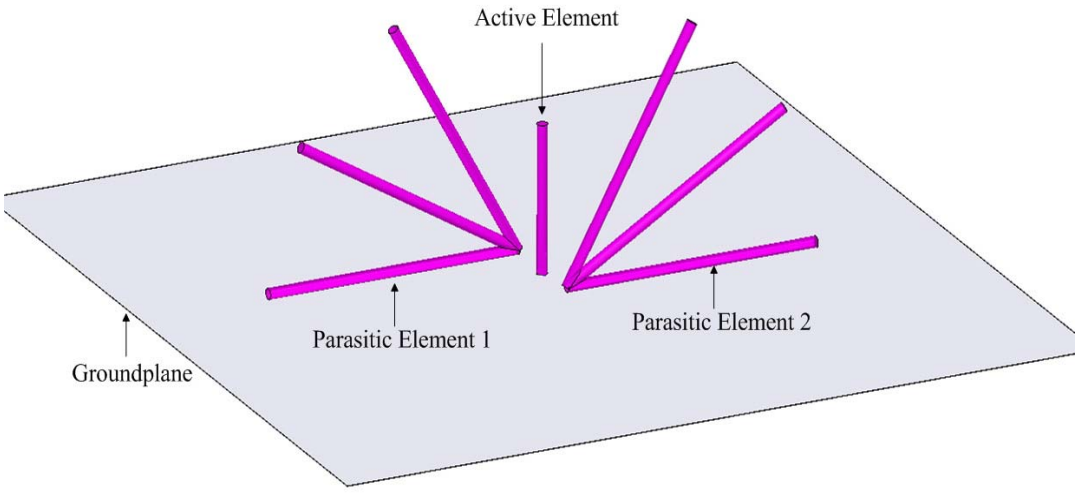

Figure 3-15 Demonstration of the antenna with Trident-Shaped parasitic elements

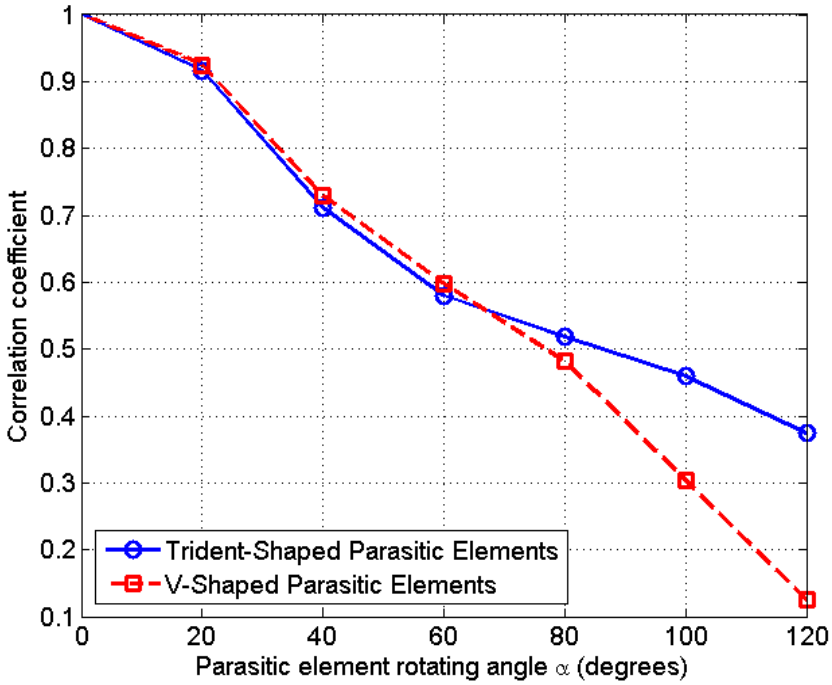

Figure 3-16 Pattern correlation coefficient of the antenna with V-Shaped parasitic elements and Trident-Shaped parasitic elements

The results show that the Trident-Shape model has a similar, or worse, diversity performance than the proposed V-shaped model, in most configurations. Therefore, adding more wire arms into the parasitic elements will not improve the diversity performance of the proposed configuration.

3.5 Conclusion

We have presented a new antenna for being able to realize diversity action. The system uses isolated wires for its parasitic elements, so that no switch or varying reactive loads are required. This removes the disadvantage of many switched parasitic element technologies. The design is simple, and is suitable for simple mechanical actuation. The technology is likely to be most useful in integrated microelectronic designs, where high frequencies allow physically small antennas that can be integrated on chips.

Results of parametric study confirmed the pattern-changing ability and diversity achieved of this model.

Other shapes of parasitic elements were also tested and compared with the proposed model. Chapter 4 will introduce a new shape of the parasitic elements by using moveable metal sheets.

4: RECONFIGURABLE ANTENNA APPLICATION (METAL PARASITIC ELEMENT)

In the previous chapter, an antenna with two wire parasitic elements (V-Shaped) is proposed. In this chapter, another shape of parasitic element will be reviewed. This shape of the parasitic element comprises a piece of metal, namely ‘Shell-Shaped’ parasitic elements, as illustrated in Figure 4.1

The V-Shaped parasitic elements comprises light materials due to the need to electronically move the parasitic elements. If the weight of the parasitic elements is less of a concern (e.g., an electrical motor can be used to drive the parasitic element), then using the Shell-Shaped parasitic elements could gain more performance in terms of diversity and pattern-changing, for a given range of rotation angles.

This chapter has the following sections. Section 4.1 provides the antenna configuration. Two of the simulated far-field patterns will be shown in Section 4.2 to illustrate the pattern changing ability. The important parameters that impact the diversity performance are discussed in Section 4.3. Section 4.4 shows the

performance of the antenna with single Shell-Shaped element. Section 4.5 concludes the results of the chapter.

4.1 Demonstration of Shell-Shaped Parasitic Elements

Similar to the antenna with V-Shaped Parasitic elements, this model comprises a quarter-wavelength monopole antenna, with two Shell-Shaped parasitic elements in opposing orientations.

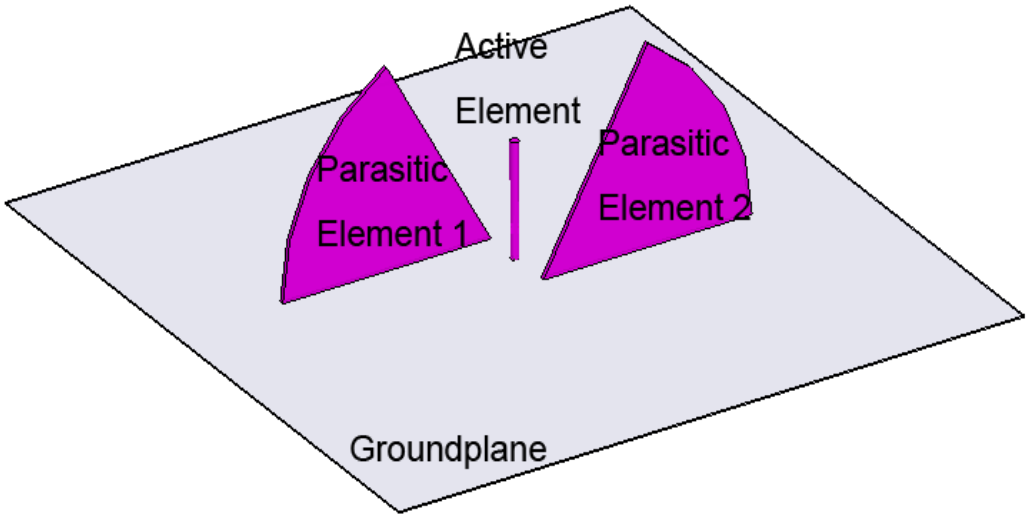

Figure 4-1 Configuration of the Shell-Shaped parasitic elements in original position

The movement of the parasitic elements in this chapter is exactly the same as the V-Shaped parasitic elements. They counter-rotate on the same axis, so

the parasitic elements loci are in parallel. The key parameter, rotating angle α, is again used to measure how far the parasitic elements are rotated, as demonstrated in Figure 4.2.

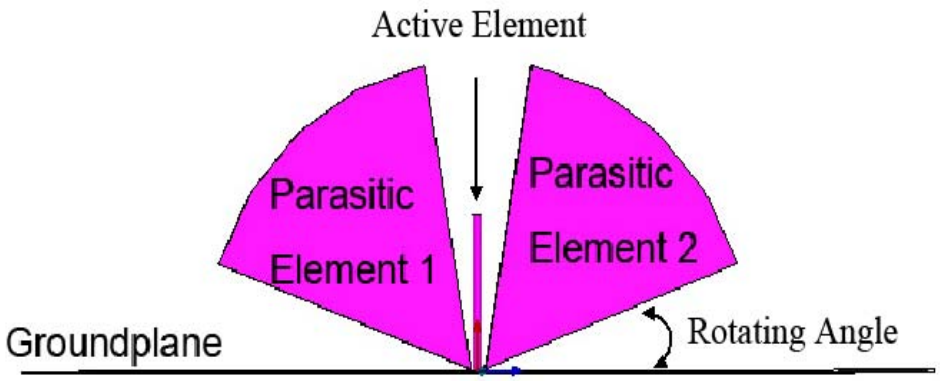

Figure 4-2 Demonstration of the movement of the Parasitic Elements

The parametric study in later sections involves the following parameters: Shell Angle (β_{shell}); Shell Length (L_{shell}); Distance between the antenna and parasitic elements (d). These parameters (except for distance d) are shown in Figure 4.3.

The groundplane size is not a critical parameter for the diversity performance as long as it is large enough. In this chapter, the groundplane size is set as 2λ.

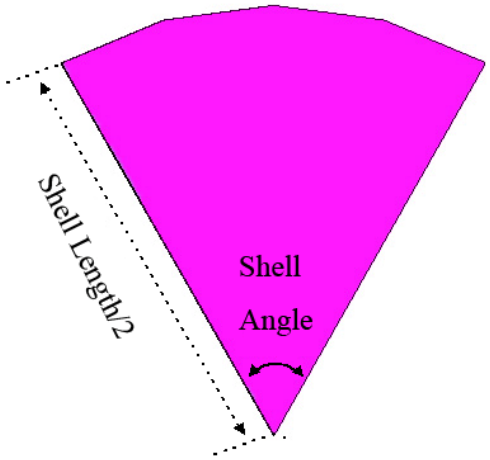

Figure 4-3 Demonstration of one single Shell-Shaped Parasitic Element

4.2 Far-field Pattern Change

The pattern change can be achieved by rotating the Shell-Shaped parasitic elements. Figure 4.4 shows the difference in antenna gain pattern (dB) when the parasitic elements are in the original position (rotating angle α=0^o) and the parasitic elements are rotated by 60^o.

Figure 4.4 is the dipole horizontal cut (θ=90^o). The change of the radiation pattern can also be observed in all other rotating angles.

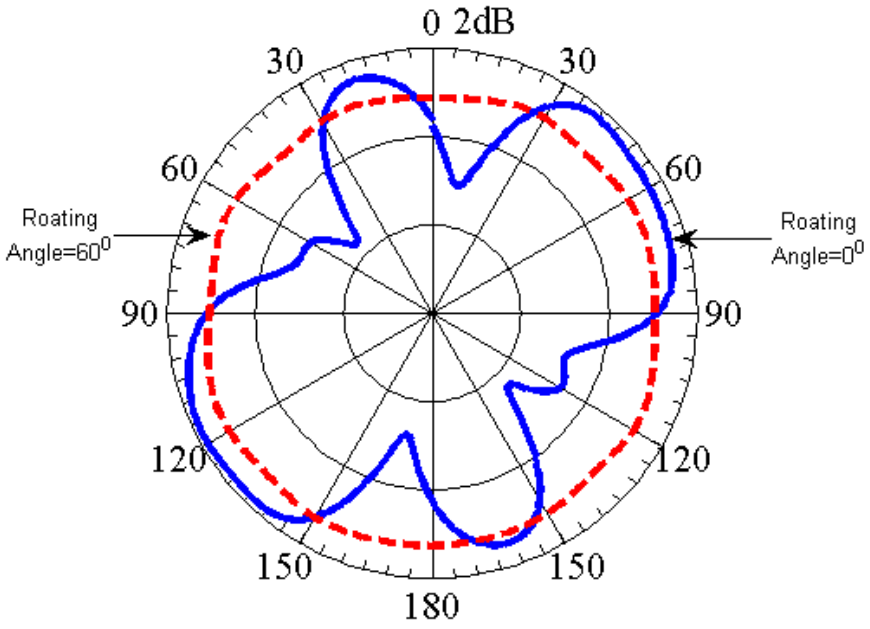

Figure 4-4 Demonstration of gain pattern change when the rotating angle=0° and 60°

There is a noticeable difference in the gain pattern between the antenna with V-Shaped parasitic element and Shell-Shaped parasitic element. The Shell-Shaped parasitic element is composed of a piece of metal sheet which will block and diffract. This creates a better pattern-changing ability.

4.3 Diversity Performance

Three important parameters mentioned in Section 4.1 are critical to the correlation coefficient. In this section, HFSS simulation results are provided with the comparison to the antenna with V-Shaped parasitic elements. Similar to the previous chapter, the correlation results are based on the pattern of the antenna when the parasitic elements are in their original position (rotating angle $\alpha=0^o$) and the pattern of the antenna with the parasitic elements at other rotation angles.

4.3.1 Shell angle

The shell angle β_{shell} is equivalent to the Bend Angle β in V-Shape model. The best choice of the V-Shaped Bend Angle is 60^o. In the Shell-Shaped model, this angle is set to be 30^o, 60^o and 90^o. Detailed simulation results can be found in Figure 4.5.

Again, the rotating angle is still bound to the shell angle. The parasitic element with the shell angle at 60^o can only rotate 120^o before it touches the other side of the groundplane.

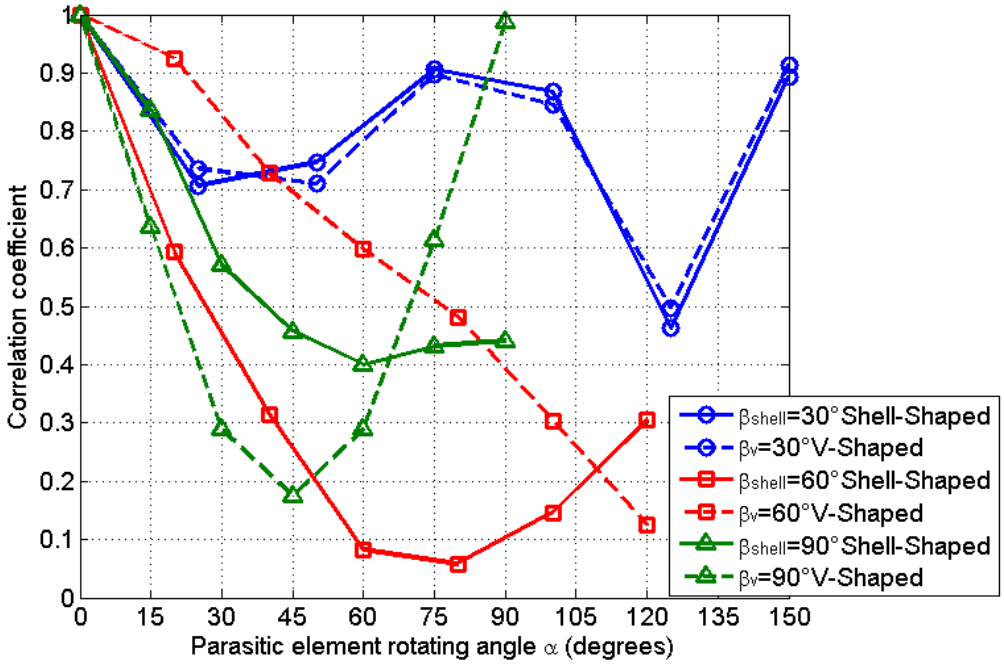

Figure 4-5 Pattern correlation coefficient of the antenna under different shell angles

From Figure 4.5, the shell angle at 60^{o} is still a good angle for the parasitic elements. The antenna with a shell angle of 30^{o}, although has the widest rotating range, has a worst diversity performance and has almost no performance difference between the V-Shaped parasitic elements. The diversity performance of the antenna with a shell angle at 90^{o} also behaves no better than the V-Shaped parasitic elements. The antenna with the shell angle at desired 60^{o} provides the best correlation coefficient value at 0.06 when the rotating angle is around 75^{o} and outperforms all antenna models in terms of diversity performance.

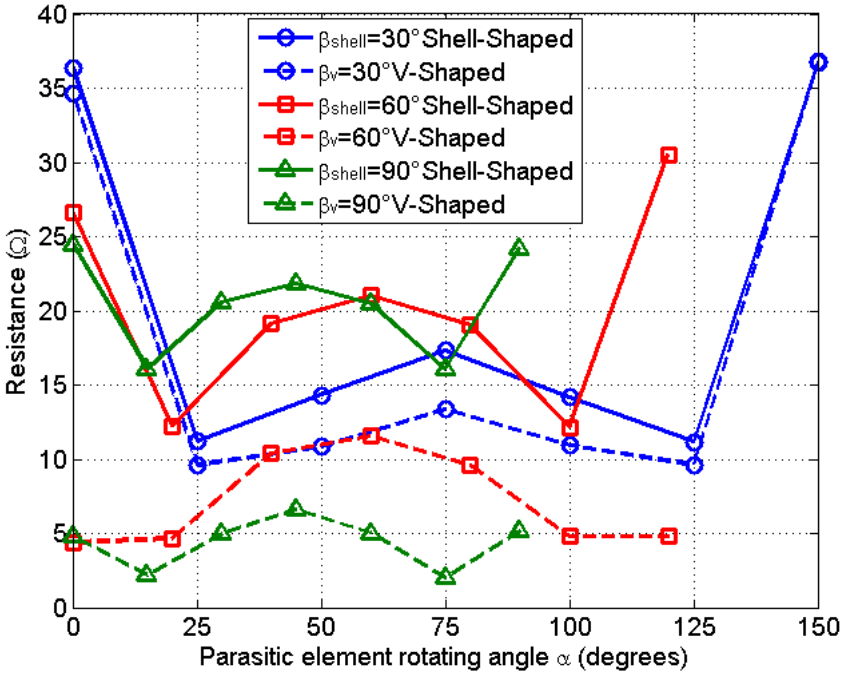

Figure 4-6 Resistance of the antenna under different shell angles

The resistance evaluation can be found in Figure 4.6. The antenna with the shell angle of 30° still behaves similar to the associated V-Shape model. With a shell angle at 60°, although the resistance fluctuates more than the V-Shape model, is generally acceptable and closer to the common feed impedance of 50Ω.

In conclusion, the desired shell angle should be 60° since it has a better diversity performance, acceptable impedance curve and a large range of rotation angle which is capable of producing more pattern changing effects.

4.3.2 Shell length

The shell length L_{shell} is equivalent to the parasitic element length in V-Shape model. It has a significant influence on the diversity performance. Such length has to be long enough to influence the radiation pattern, yet if the length is too long, the antenna becomes less compact. Therefore, a parametric study is necessary to achieve the lowest correlation using smallest shell length. Results are demonstrated in Figure 4.7 and 4.8.

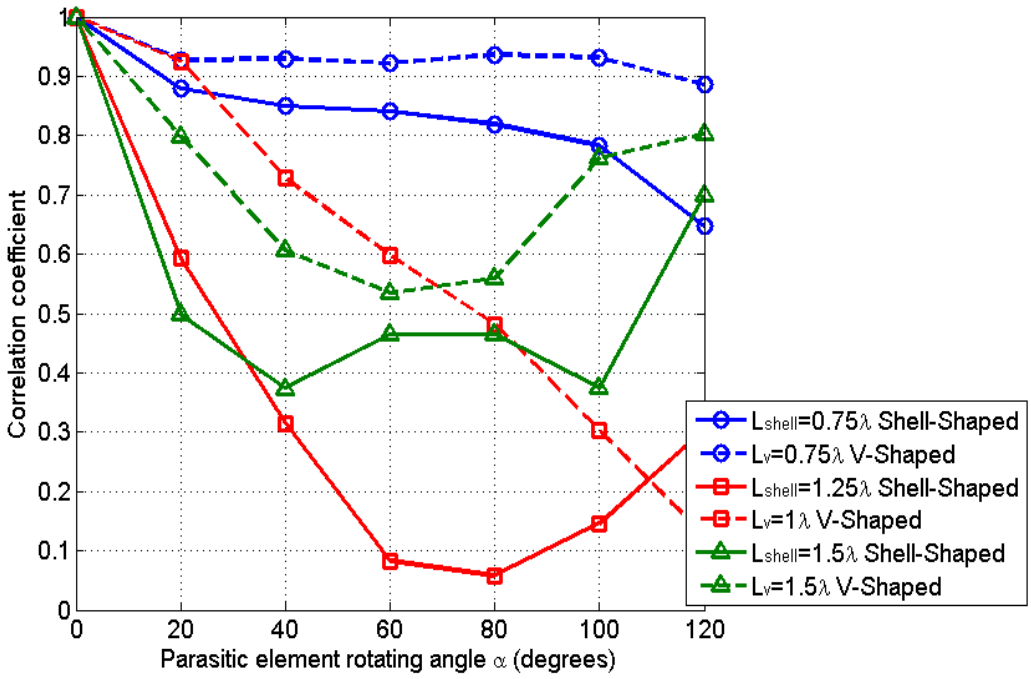

Figure 4-7 Pattern correlation coefficient of the antenna under different shell lengths

Figure 4.7 shows the correlation coefficient results obtained by changing shell lengths. Obviously the antenna with the parasitic elements at 0.75λ is too short to influence the far-field pattern. This conclusion has already been proposed in the V-Shaped model. The antenna with the parasitic elements of length 1.5λ does not have a good diversity action, despite the antenna dimension being bigger. Different lengths, such as 2λ, are also simulated, and the results (not shown) are similar to the antenna with the parasitic elements lengths of 1.5λ

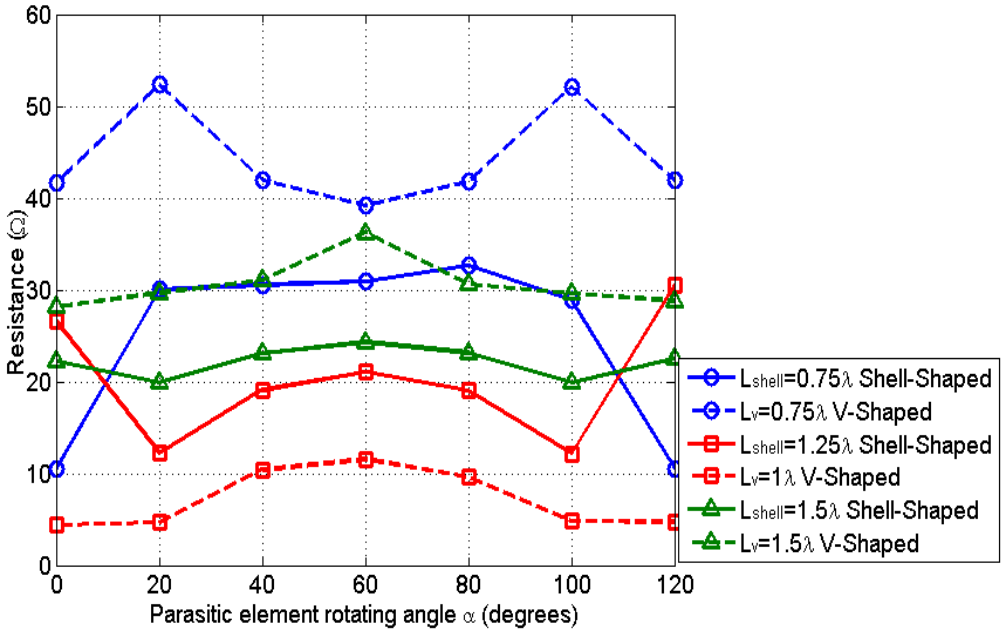

Figure 4-8 Resistance of the antenna under different shell length

The impedance behaviour is less informative than the correlation performance. Changing the length of the parasitic elements does not provide significantly changed impedance.

The antenna with the parasitic element at 1λ apparently outperformed all other antenna models with other lengths of parasitic elements. Therefore, the best option for the parasitic elements length should be 1λ.

4.3.3 Distance between antenna and parasitic elements

The distance *d* in this sub-section is defined as the distance between antenna and parasitic elements. This distance is a critical parameter since it directly affects the radiation pattern. Simulated correlation results are in Figure 4.9.

The antenna with a distance separating active and parasitic elements at 0.05λ brings no contribution to the correlation in V-Shape model. However in the Shell-Shape model, it has a relatively acceptable diversity performance. From the figure, apparently the antenna with a separating distance at 0.1λ distance behaves much better. It provides the lowest correlation coefficient of the other distances in the figure.

For the resistance, the antenna with separating distance at 0.2λ gives a varying curve. The conclusion can be drawn that the range of distance between the active and parasitic elements of 0.05λ and 0.2λ impacts the radiation since the impedance fluctuates, but the diversity performance is not good. Overall, the separating distance at 0.1λ is still a good choice.

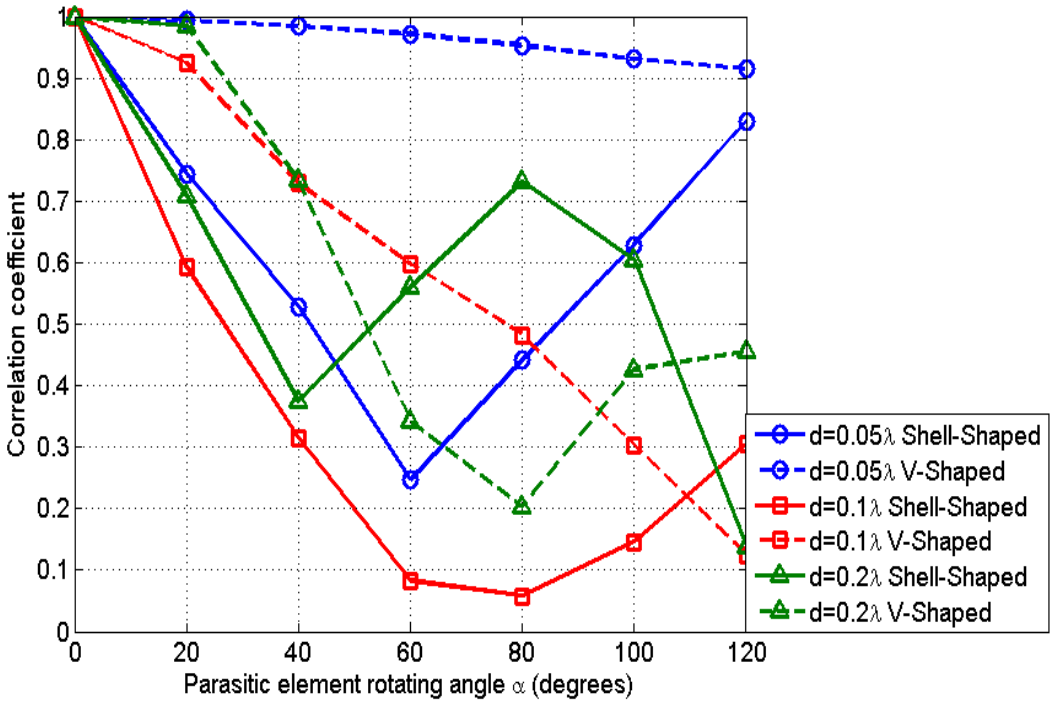

Figure 4-9 Pattern correlation coefficient of the antenna under different distance

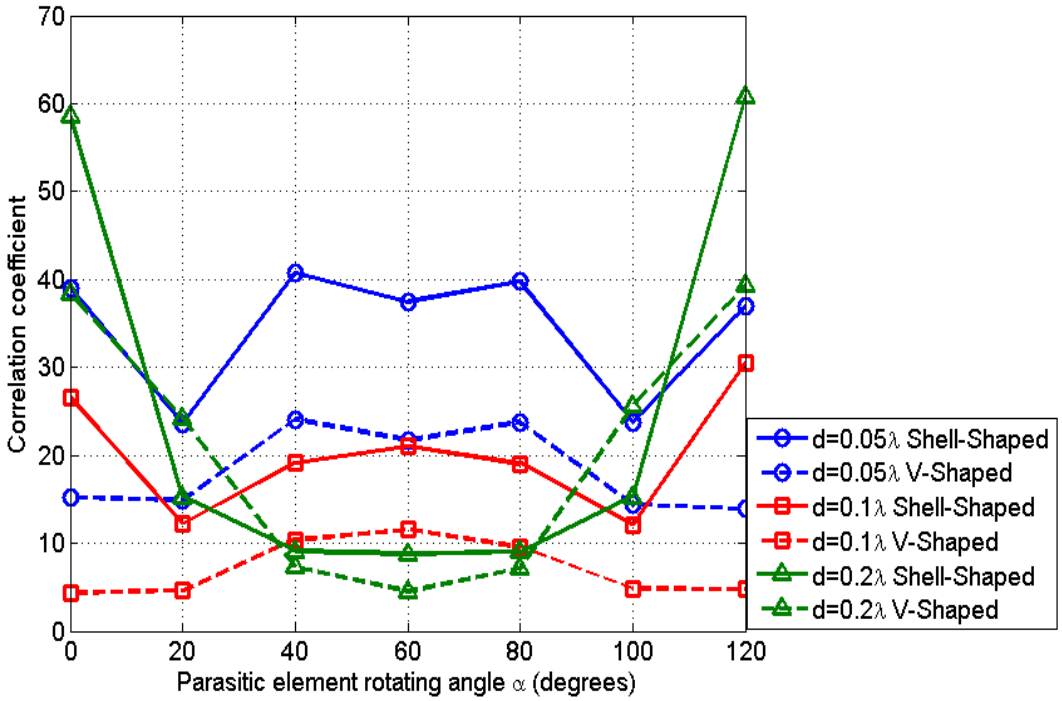

Figure 4-10 Resistance of the antenna under different distance

4.3.4 Recommended value of each parameter

A good choice of parameters are given in Table D.

TABLE D Recommended parameter values for the reconfigurable antenna with sheet parasitic elements

Symbol	***Definition***	***Value***
β_{shell}	Shell Angle	60^{o}
d	Distance between antenna and parasitic elements	0.1λ
L_{shell}	Length of the parasitic elements	1λ

4.4 Single Shell-Shaped Parasitic Element

The results of the dual Shell-Shaped elements demonstrated diversity action. A single Shell-Shape antenna, shown in Figure 4.11, has also been simulated.

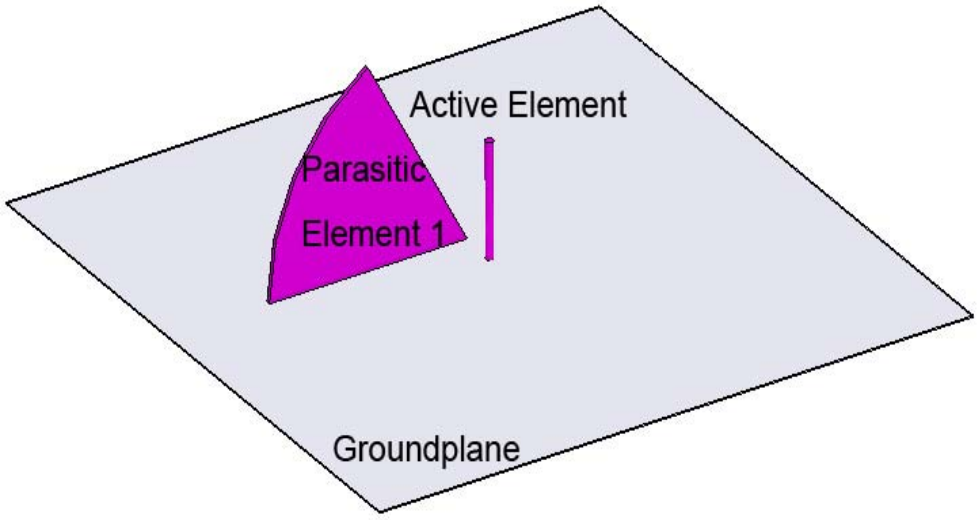

Figure 4-11 Demonstration of the antenna with single Shell-Shaped parasitic element

The objective for this model is still the pattern-changing ability and diversity performance. The gain pattern in horizontal cut ($\theta=90^{o}$) is provided in Figure 4.12.

Apparently, the pattern changing ability is still good, with one parasitic element eliminated. It can also be observed from the figure that the horizontal

gain is increased by 2.5dBi compared to the antenna with two Shell-Shaped parasitic elements.

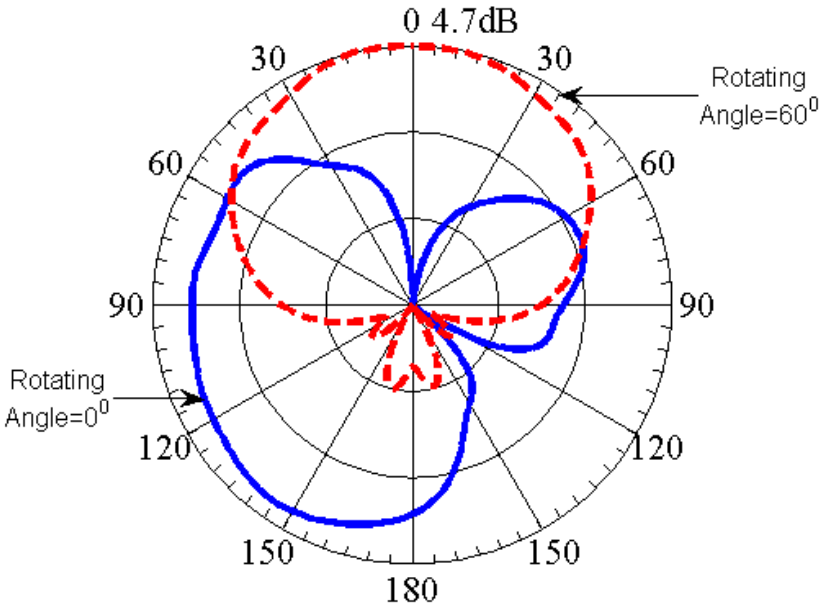

Figure 4-12 Demonstration of gain pattern change for single Shell-Shaped parasitic element when the rotating angle =0° and 60°.

The correlation results for this antenna is in Figure 4.13. With the single parasitic element, the correlation performance is not as good as the antenna with dual parasitic elements, although the lowest correlation coefficient is around 0.2.

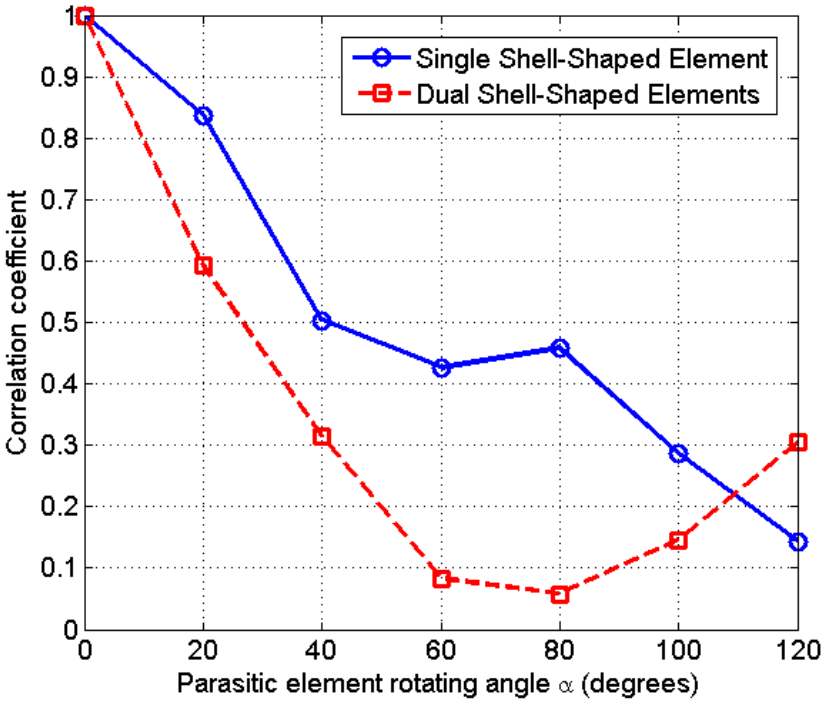

Figure 4-13 Pattern correlation coefficient comparison between dual and single Shell-Shaped parasitic element(s)

The antennas with both single Shell-Shaped parasitic element and dual Shell-Shaped parasitic elements provide good pattern-changing ability and correlation results. Overall, the configuration with dual parasitic elements is more effective in changing the pattern and better in diversity performance.

4.5 Conclusion

In this chapter, the parasitic element has been revised to be Shell-Shaped metal sheets. The pattern changing ability and associated diversity performance are improved compared to the V-shaped parasitic designs of Chapter 3. But because the design requires larger (i.e. heavier) parasitic elements, their actuation would be more complex.

5: CONCLUSION AND FUTURE WORK

A new type of diversity antenna has been developed. It uses moving parasitic elements and a fixed active element. Through electromagnetic simulation, the electrical configuration has been derived and its performance demonstrated. Pattern correlation indicates that the antenna has good diversity performance. The antenna, being mechanically reconfigurable, is for slowly changing scenarios. Likely applications for future systems are for integrated design on chips, with frequencies above 40GHz. Detailed simulation results are provided, and the accuracy of the simulation software is also verified through different simulation and measurement using an elementary dipole antenna.

Suggestions for Future Research

The behaviour of the parasitic wires in very close proximity (0.05 wavelengths) shows little impact on the pattern. This is not an obvious result, but it is likely that the coupling is so strong that all the wires have essentially the same currents. This should be investigated by looking at all the currents on the

antenna. Simulation packages are reliable for finding these currents, and confirming this idea.

A mechanically reconfigurable antenna following the designs presented here has been built by K. Daheshpour [29]. The configurations with the Shell-Shaped parasitic elements look promising for implementation on chips, and SFU has capability in implementing this. It would be of interest to develop a 60GHz prototype with integrated electronic actuation.

Further configurations beckon. One promising idea is to use a corner-type reflector to increase the pattern-changing action as well as the antenna gain.

REFERENCE LIST

[1] Adams, A.T., Warren, D.E., “Dipole plus parasitic element,” *IEEE Trans. Antennas Propagation*, Vol. AP-19, pp. 536–537, July 1971.

[2] Harrington, R.F., “Reactively controlled directive arrays,” *IEEE Transactions on Antennas and Propagation*, vol. 26, pp. 390–395, May 1978.

[3] Milne, R.M.T. “A small adaptive array antenna for mobile communications,” *IEEE Antennas and Propagation Society Symposium Dig*est, pp. 797-800, June 1985.

[4] Preston, S.L., Thiel, D.V., Smith, T.A., O’Keefe, S.G., and Lu, J.W.,“Base-station tracking in mobile communications using a switched parasitic antenna array*”, IEEE Transactions on Antennas and Propagation*, Vol. 46, No. 6, pp.841-844, June 1998.

[5] Dinger, R.J., “Reactively steered adaptive array using microstrip patch elements at 4GHz,” *IEEE Transactions on Antennas and Propagation*, vol. 32, pp. 848–856, August 1984.

[6] Preston, S.L., Thiel, D.V., Lu, J.W., O’Keefe, S.G., and Bird, T.S., “Electronic beam steering using switched parasitic patch elements,” *Electronics Letters*, Vol. 33, Issue. 1, pp.7–8, Jan. 1997.

[7] Vaughan, R. G., “Switched parasitic elements for antenna diversity,” *IEEE Transactions on Antennas and Propagation*, Vol. 47, No.2 , pp.399-405, Feb. 1999.

[8] Scott, N.L., Leonard-Taylor, M., Vaughan, R.G., “Diversity gain from a single-port adaptive antenna using switched parasitic elements illustrated with a wire and monopole prototype” *IEEE Trans. Antennas and Propagat*ion, Vol. 47, No.6 , pp.1066-1070, Jun. 1999.

[9] Clarricoats, P.J.B., Monk, A.D., Zhou, H., “Array-fed reconfigurable reflector for spacecraft systems,” *Electronic Letters*, Vol.30, Issue.8, pp. 613-614, April 1994.

[10] Bernhard, J.T., *Reconfigurable Antennas*, Morgan and Claypool, 2007.

[11] Mahanfar, N., Menon, C., Vaughan, R.G., “Smart antennas using electro-active polymers for deformable parasitic elements”, *Electronic Letters*, Vol. 44, Issue 19, p.1113–1114, 11 Sept. 2008.

[12] W.D. Rawle, " The Method of Moments: A Numerical Technique for Wire Antenna Design," *High Frequency Electronics*, Feb.2006.

[13] R. Vaughan and J. Andersen, *Channels, Propagation and Antennas for Mobile Communications*, 1st ed. London, United Kingdom: Institution of Electrical Engineers, 2003.

[14] D. Otto, “A note on the induced EMF method for antenna impedance, ”*Antennas and Propagation, IEEE Transactions on [legacy, pre-1988]*, vol. 17, no. 1, pp. 101–102, 1969.

[15] K. K. Mei, “On the integral equations of thin wire antennas,” *IEEE Trans. Antennas Propagation.* vol.AP-13, pp.374–378, May 1965.

[16] C. M. Butler and D. R. Wilton, “Analysis of various numerical techniques

applied to thin-wire scatterers,” *IEEE Trans. Antennas Propagation,* vol. AP-23, pp. 534–540, July 1975.

[17] R. F. Harrington, *Field Computation by Moment Methods*. New York:

Macmillan, 1968.

[18] DH Werner, “A method of moments approach for the efficient and accurate modeling of moderately thick cylindrical wire antennas,“ *IEEE Trans. Antennas Propagation,* vol.46, pp.373-381, March 1998.

[19] P. G. Rogers and M. W. Gunn, “An entire-domain Galerkin analysis of the moderately thick dipole,” *IEEE Trans. Antennas Propagation*, vol.AP-28, pp.117–121, Jan. 1980.

[20] H. Grandin, *Fundamentals of the Finite Element Method*. MacMillan,1986.

[21] A. Taflove and K. Umashankar, “The Finite-Difference Time-Domain Method for Numerical Modeling of Electromagnetic Wave Interactions,” *Electromagnetics*, vol. 10, no. 1, pp. 105–126, 1990.

[22] D. S. Katz *et al.,* “FDTD analysis of electromagnetic wave radiation from systems containing horn antennas,” *IEEE Trans. Antennas Propagation,* vol. 39, pp. 1203-1212, Aug. 1991.

[23] R. Luebbers and K. Kunz, “Finite difference time domain calculations of antenna mutual coupling,” *IEEE Trans. Electromagn.Compat.,* vol. 34, pp. 357-360, Aug. 1992.

[24] C. Balanis, *Antenna Theory: Analysis and Design*, 3rd ed. Hoboken, New Jersey, USA: John Wiley & Sons, Inc., 2005.

[25] W. L. Stutzman and G. A. Thiele, *Antenna theory and design*, 1981.

[26] S. Bhattacharya, S. A. Long, and D. R. Wilton, “The input impedance of a monopole antenna mounted on a cubical conducting box,” *IEEE Trans. Antennas Propagation,* ” vol. AP-35, pp. 756-762, July 1987.

[27] A. Chu, S. A. Long, and D. R. Wilton, “The radiation pattern of a monopole antenna attached to a conducting box,” *IEEE Trans. Antennas Propagation,*” vol. 38, pp. 1907-1912, Dec. 1990.

[28] AS Meier, WP Summers, "Measured Impedance of Vertical Antennas Over Finite Ground Planes, " *Proceedings of the IRE*, 1949.

[29] K. Daheshpour, Master Thesis, Simon Fraser University.